

HIGH TEMPERATURE PROTON EXCHANGE MEMBRANE FUEL
CELLS

A THESIS SUBMITTED TO
THE GRADUATE SCHOOL OF NATURAL AND APPLIED
SCIENCES
OF
MIDDLE EAST TECHNICAL UNIVERSITY

BY

DİLEK ERGÜN

IN PARTIAL FULFILLMENTS OF THE REQUIREMENTS
FOR
THE DEGREE OF MASTER OF SCIENCE
IN
CHEMICAL ENGINEERING

AUGUST 2009

Approval of the thesis

**HIGH TEMPERATURE PROTON EXCHANGE MEMBRANE
FUEL CELLS**

submitted by DİLEK ERGÜN in partial fulfillment of the requirements
for the degree of **Master of Science in Chemical Engineering**
Department, Middle East Technical University by,

Prof. Dr. Canan Özgen
Dean, Graduate School of **Natural and Applied Sciences** _____

Prof. Dr. Gürkan Karakaş
Head of Department, **Chemical Engineering** _____

Prof. Dr. İnci Eroğlu
Supervisor, **Chemical Engineering Dept., METU** _____

Prof. Dr. Nurcan Baç
Co-supervisor, **Chemical Engineering Dept.,
Yeditepe University** _____

Examining Committee Members:

Prof. Dr. Erdoğan Alper
Chemical Engineering Dept., Hacettepe University _____

Prof. Dr. İnci Eroğlu
Chemical Engineering Dept., METU _____

Prof. Dr. Nurcan Baç
Chemical Engineering Dept., Yeditepe University _____

Assistant Prof. Dr. Serkan Kıncal
Chemical Engineering Dept., METU _____

Dr. Ayşe Bayrakçeken
Chemical Engineering Dept., Atatürk University _____

Date: 03.08.2009

I hereby declare that all information in this document has been obtained and presented in accordance with academic rules and ethical conduct. I also declare that, as required by these rules and conduct, I have fully cited and referenced all material and results that are not original to this work.

Name, Last name : DİLEK ERGÜN

Signature :

ABSTRACT

HIGH TEMPERATURE PROTON EXCHANGE MEMBRANE FUEL CELLS

Ergün, Dilek

M.S., Department of Chemical Engineering

Supervisor: Prof. Dr. İnci Eroğlu

Co-Supervisor: Prof. Dr. Nurcan Baç

August 2009, 97 pages

It is desirable to increase the operation temperature of proton exchange membrane fuel cells above 100°C due to fast electrode kinetics, high tolerance to fuel impurities and simple thermal and water management.

In this study; the objective is to develop a high temperature proton exchange membrane fuel cell. Phosphoric acid doped polybenzimidazole membrane was chosen as the electrolyte material. Polybenzimidazole was synthesized with different molecular weights (18700-118500) by changing the synthesis conditions such as reaction time (18-24h) and temperature (185-200°C). The formation of polybenzimidazole was confirmed by FTIR, H-NMR and elemental analysis. The synthesized polymers were used to prepare homogeneous membranes which have good mechanical strength and high thermal stability. Phosphoric acid doped membranes were used to prepare membrane electrode assemblies.

Dry hydrogen and oxygen gases were fed to the anode and cathode sides of the cell respectively, at a flow rate of 0.1 slpm for fuel cell tests. It was achieved to operate the single cell up to 160°C. The observed

maximum power output was increased considerably from 0.015 W/cm² to 0.061 W/cm² at 150°C when the binder of the catalyst was changed from polybenzimidazole to polybenzimidazole and polyvinylidene fluoride mixture. The power outputs of 0.032 W/cm² and 0.063 W/cm² were obtained when the fuel cell operating temperatures changed as 125°C and 160°C respectively. The single cell test presents 0.035 W/cm² and 0.070 W/cm² with membrane thicknesses of 100 μm and 70 μm respectively. So it can be concluded that thinner membranes give better performances at higher temperatures.

Keywords: polybenzimidazole, polymer electrolyte, membrane electrode assembly, proton exchange membrane fuel cell

ÖZ

YÜKSEK SICAKLIKTA ÇALIŞABİLEN PROTON DEĞİŞİM ZARLI YAKIT HÜCRELERİ

Ergün, Dilek

Y.L., Kimya Mühendisliği Bölümü

Tez Yöneticisi: Prof. Dr. İnci Eroğlu

Ortak Tez Yöneticisi: Prof. Dr. Nurcan Baç

Ağustos 2009, 97 sayfa

Proton değişim zarlı yakıt hücrelerinin çalışma sıcaklıklarının 100°C üzerine çıkarılması; hızlı elektrot kinetiği, yakıt safsızlıklarının toleransı, kolay ısı ve su yönetimi gibi avantajlardan dolayı tercih edilir.

Bu çalışmada amaç; yüksek sıcaklıkta çalışabilen proton değişim zarlı bir yakıt pili geliştirmektir. Elektrolit malzemesi olarak; fosforik asit yüklü polibenzimidazol membran seçilmiştir. Reaksiyon süresi (18-24 saat) ve sıcaklığı (185-200°C) gibi sentez koşulları değiştirilerek farklı molekül ağırlıklarında (18700-118500) polimerler sentezlenmiştir. Polibenzimidazolun oluşumu FTIR, H-NMR ve elementel analiz ile doğrulanmıştır. Sentezlenen polimerler iyi mekanik dayanım ve yüksek ısıl kararlılığa sahip homojen membranlar hazırlamak için kullanılmıştır. Fosforik asit ile yüklenen membranlar membran elektrot ataçları hazırlamak için kullanılmıştır.

Yakıt pili testleri için, hücrenin anot ve katot bölümlerine sırasıyla kuru hidrojen ve oksijen gazları 0.1 slpm hızda beslenmiştir. Tek hücrenin 160°C sıcaklığa kadar çalıştırılması başarılmıştır. Katalizör iyonomeri

polibenzimidazolden polibenzimidazol -polivinylidene fluorid karışımına değiştirildiğinde; 150°C'de gözlemlenen güç çıkışı 0.015W/cm²'den 0.061 W/cm²'ye çıkmıştır. Yakıt pili işletim sıcaklığı 125°C ve 160°C'ye değiştirildiğinde ise güç çıkışları sırasıyla 0.032W/cm² ve 0.063W/cm² olarak elde edilmiştir. Tek hücre testleri 100µm ve 70µm kalınlığındaki membranlarla yapıldığında; sırasıyla 0.035W/cm² ve 0.070W/cm² maksimum güç çıkışları vermiştir. Dolayısıyla daha ince membranların yüksek sıcaklıklarda daha iyi performans verdiği sonucuna ulaşılmıştır.

Anahtar Kelimeler: polibenzimidazol, polimer elektrolit, membran elektrot atacı, proton değim zarlı yakıt pili

To my family

ACKNOWLEDGEMENT

I would like to express my sincere gratitude to my supervisor Prof. Dr. İnci Erođlu for her guidance, criticism, encouragements and also sharing her immense knowledge with me throughout the research.

I would also like to thank my co-supervisor Prof. Dr. Nurcan Ba for his suggestions, comments and guidance.

I would like to express the deepest appreciation to Dr. Yılser Devrim for her helpful discussions in polymer science and also suggestions and encouragements in every stage of my experiments throughout the research.

My special thanks go to my lab mate Serdar Erkan who was always helpful to me in finding solutions to unexpected problems I face. This study would be much more challenging without his explanations, experiences and also friendship.

Appreciations also go to Berker Fııcılar, Dr. Aye Bayrakeken, Burcu Gvenatam and all fuel cell research group members for their contributions to my study and also their kind cooperation in the lab.

I am indebted to my family for their endless support, help, motivation and being with me all time. I also thank to my friends; İnci Ayrancı and Hatice afak Bozkır for their encouragement and sincere friendship.

This study was supported by TUBITAK with project 104M364 and METU BAP-2008-03-04-07.

TABLE OF CONTENTS

ABSTRACT	iv
ÖZ.....	vi
ACKNOWLEDGEMENT.....	ix
LIST OF FIGURES.....	xiv
LIST OF TABLES	xvii
LIST OF SYMBOLS.....	xviii
CHAPTERS	
1. INTRODUCTION.....	1
2. PROTON EXCHANGE MEMBRANE FUEL CELLS.....	9
2.1. Principles of Proton Exchange Membrane Fuel Cells.....	9
2.2. Main Components of Proton Exchange Membrane Fuel Cells	11
2.2.1. Electrolyte: Membrane.....	12
2.2.2. Electrodes and Gas Diffusion Layers.....	14
2.2.3. Bipolar plates	16
2.2.4. Gaskets	16
2.3. Operation of PEM Fuel Cell.....	17
2.3.1. Fuel Cell Electrochemistry and Polarization Curve.....	17
2.3.2. Effect of Temperature on Theoretical Cell Potential	23
2.3.3. High Temperature Operation of PEMFC.....	24
2.4. High Temperature Proton Exchange Membranes.....	25
2.5. General Information about Polybenzimidazoles	26

2.5.1. Synthesis of PBI.....	27
2.5.2. Phosphoric Acid Doped PBI Membranes and Proton Conduction Mechanism	28
3. EXPERIMENTAL	32
3.1. Preparation of Phosphoric Acid Doped Polybenzimidazole Membranes	32
3.1.1. Materials.....	32
3.1.2. Polybenzimidazole Synthesis.....	33
3.1.3. Membrane Preparation.....	36
3.1.4. Acid Doping of the Membranes.....	37
3.2. Characterization of Polybenzimidazole Polymer	37
3.2.1 Nuclear Magnetic Resonance Spectra.....	37
3.2.2. Fourier Transform Infrared Spectroscopy.....	38
3.2.3. Elemental Analysis	38
3.2.4. Determination of Molecular Weight.....	38
3.3. Characterization of the membranes	40
3.3.1. Fourier Transform Infrared Spectroscopy.....	40
3.3.2. Thermogravimetric analysis.....	40
3.3.3. X- Ray Diffraction Analysis	41
3.3.4. Mechanical analysis	41
3.4. Preparation of Membrane Electrode Assembly.....	41
3.4.1. Membrane Electrode Assembly Preparation Technique.....	41
3.4.2. Surface Morphology of the Electrodes	44
3.5. PEMFC Performance Tests	44

3.6. Scope of the Experiments	47
4. RESULTS AND DISCUSSION	51
4.1. Characterization of PBI Polymer.....	51
4.1.1. Nuclear Magnetic Resonance Spectra.....	51
4.1.2. Fourier Transform Infrared Spectroscopy.....	52
4.1.3. Elemental Analysis	53
4.1.4. Molecular Weight	54
4.2. Characterization of PBI Membrane.....	58
4.2.1. Fourier Transform Infrared Spectroscopy.....	58
4.2.2. X-Ray Diffraction Analysis	61
4.2.3. Thermal characteristics of PBI membranes	63
4.2.4. The Mechanical Strength of the Membranes	65
4.3. Surface Morphology of the Electrodes	67
4.3.1. Scanning Electron Microscopy and Energy Dispersive X-ray Analysis of the Electrode Surface.....	68
4.3.2. Scanning Electron Microscopy Analysis of the MEA Cross Sections	71
4.4. PEMFC Performance Tests	74
4.4.1. Effect of binder used in the catalyst ink on PEMFC Performance	75
4.4.2. Effect of Temperature on PEMFC Performance.....	77
4.4.3. Effect of Membrane Thickness on PEMFC Performance	78
4.4.4. The Effect of Operating Time on Fuel Cell Performance.....	79
4.5. Summary of the PEM Fuel Cell Performance Analysis	81

5. CONCLUSIONS AND RECOMMENDATIONS.....	83
REFERENCES	88
APPENDIX A	95
APPENDIX B.....	96

LIST OF FIGURES

FIGURES

Figure 1.1 Fuel cell diagram.....	3
Figure 2.1 Diagram of PEM fuel cell principle.....	10
Figure 2.2 Main components of PEMFC.....	12
Figure 2.3 Typical polarization curve for fuel cell with significant losses.....	23
Figure 2.4 Reaction scheme of PBI by melt polycondensation.....	28
Figure 2.5 Reaction scheme of PBI by solution polymerization.....	28
Figure 2.6 Proton conduction mechanism of H ₃ PO ₄ doped PBI (a) Acid bi acid interaction (b) Acid acid interaction.....	31
Figure 3.1 Reaction scheme of PBI synthesis.....	33
Figure 3.2 The picture of the experimental set up for PBI synthesis.....	34
Figure 3.3 The picture of the purification procedure.....	35
Figure 3.4 PBI membrane preparation a) PBI powder b) Membrane solution c) PBI membrane.....	36
Figure 3.5 The experimental set up of viscosity measurement.....	40
Figure 3.6 Flow charts of MEA preparation.....	43
Figure 3.7 Single PEM fuel cell.....	45
Figure 3.8 Schematic representation of fuel cell test station.....	46
Figure 3.9 The picture of the PEM fuel cell test station.....	47
Figure 3.10 Flow chart of the experiments.....	49
Figure 4.1 H-NMR spectra of the synthesized PBI.....	52
Figure 4.2 FTIR spectra of PBI.....	53
Figure 4.3 Concentration vs viscosity plot.....	55
Figure 4.4 PBI membrane that is cast from the polymer with a molecular weight of < 18000.....	56

Figure 4.5 FTIR spectra of a) PBI membrane b) H ₃ PO ₄ doped PBI membrane.....	60
Figure 4.6 XRD patterns of (a) undoped and (b) H ₃ PO ₄ doped PBI membranes.....	62
Figure 4.7 TGA spectra of (a) pristine PBI membrane (b) H ₃ PO ₄ doped PBI membrane.....	64
Figure 4.8 Stress at break values of the PBI membranes for different doping levels and molecular weights.....	66
Figure 4.9 Stress-strain curves of the PBI membranes that have different acid doping levels.....	67
Figure 4.10 SEM images of non-doped electrode surface (a) with a magnification of (x100) (b) with a magnification of (x50000) (electrodes prepared with 1st procedure).....	69
Figure 4.11 SEM images of H ₃ PO ₄ doped electrode surface (a) with a magnification of (x100) (b) with a magnification of (x50000) (electrodes prepared with 1st procedure).....	69
Figure 4.12 SEM images of non-doped electrode surface in which PVDF was used as a binder (a) with a magnification of (x100) (b) with a magnification of (x50000) (electrodes prepared with 2nd procedure)..	70
Figure 4.13 The EDX image of the distribution of Pt on electrode surface.....	70
Figure 4.14 SEM scans of the cross sections of the unused MEAs (a) in secondary electron (b) in backscattered mode.....	72
Figure 4.15 SEM scans of the cross sections of the MEAs after testing in PEMFC (a) in secondary electron (b) in backscattered mode.....	73
Figure 4.16 SEM scans of the cross sections of the MEAs after testing in PEMFC in backscattered mode (a) deformation occurred on the catalyst layer (b) deformation occurred on the membrane cross section.....	73

Figure 4.17 PBI performance curves at 150°C (polarization closed symbols; power-open symbols) for electrodes doped by 50% H ₃ PO ₄ and for electrodes doped by 85% H ₃ PO ₄	75
Figure 4.18 PBI performance curves (polarization closed symbols; power-open symbols) of the electrodes with a binder of PVDF:PBI= 1:3; PVDF:PBI= 1:1; PVDF:PBI= 3:1 (at 150°C).....	77
Figure 4.19 PBI performance curves (polarization closed symbols; power-open symbols) for different temperatures: 125°C; 150°C; 160°C.....	78
Figure 4.20 PBI performance curves (polarization closed symbols; power-open symbols) of the membranes with a thickness of: 100µm; 80 µm; 70µm (at 150°C).....	79
Figure 4.21 Fuel cell performances changing by time.....	80
Figure A.1 Doping level changing by time.....	95

LIST OF TABLES

TABLES

Table 1.1. Main differences of the fuel cell types.....	4
Table 2.1. Enthalpies, entropies and Gibbs free energy for hydrogen oxidation process (at 25°C).....	18
Table 2.2. Enthalpy, Gibbs free energy and entropy of hydrogen/oxygen fuel cell reaction with temperature and resulting theoretical potential (Barbir, 2005).....	19
Table 2.3 The differences between the synthesis methods of PBI (Olabisi et.al., 1996).....	27
Table 3.1 Test Conditions of performed experiments for fuel cell performance tests.....	50
Table. 4.1. The theoretical and experimental values of C, H, N elements in a PBI repeating unit(1 PBI repeating unit:308 g/mol).....	54
Table 4.2. Reaction conditions, molecular weight and intrinsic viscosities of PBI.....	56
Table 4.3. Reproducibility data of intrinsic viscosities.....	58
Table 4. 4 Test Conditions and output data of performed experiments for fuel cell performance tests (*The darkened lines are the preferable conditions.).....	82

LIST OF SYMBOLS

AFC: alkaline fuel cell
DAB: diaminobenzidine
DAB.4HCl.2H₂O: diaminobenzidine tetrahydrochloride
DI: de-ionized
DMAc: N,N-dimethylacetamide
EDX: Energy dispersive X-ray analysis
FC: fuel cell
FTIR: Fourier transform infrared spectroscopy
GDL: gas diffusion layer
IPA: isophthalic acid
MEA: membrane electrode assembly
MCFC: molten carbonate fuel cell
PBI: polybenzimidazole(poly[2,2'-(m-phenylene)-5,5'-bibenzimidazole])
NMR: nuclear magnetic resonance
PAFC: phosphoric acid fuel cell
sPEEK: sulfonated polyetheretherketone
PEM: polymer electrolyte membrane
PEMFC: proton exchange (polymer electrolyte) membrane fuel cell
PFSA: perflorosulfonic acid
PPA: polyphosphoric acid
PVDF: polyvinylidene fluoride
RH: relative humidity
RU: repeating unit
SEM: scanning electron microscopy
SOFC: solid oxide fuel cell
TGA: thermogravimetric analysis

α : transfer coefficient [dimensionless]

ΔG : change in Gibbs free energy due to the electrochemical reaction
[J/mol]

ΔV_{act} : activation polarization [V]

ΔV_{conc} : concentration polarization [V]

ΔV_{ohm} : ohmic losses [V]

η_{inh} : inherent viscosity [dl/g]

η_{int} : intrinsic viscosity [dl/g]

η_{red} : reduced viscosity [dl/g]

η_{rel} : relative viscosity [dimensionless]

η_{sp} : specific viscosity [dimensionless]

CHAPTER 1

INTRODUCTION

There is no doubt that energy demand is increasing continuously due to developing technologies, growth in population and modernized societies. Fossil fuels are the primary energy sources of the world since many years. But they will run out sooner or later as they are limited energy sources. And also burning fossil fuels to obtain energy emits greenhouse gases. So it is a must to find new energy sources for the world's demand since fossil fuels cannot be counted on in the future. This foresight leads renewable energy sources to become the main focus of recent researches. The intensive research and development studies not only promise to provide energy to improve the living standards of human beings, but also become a way out for the countries which do not have natural energy sources.

One of the most important candidates for energy production in the 21st century is hydrogen as an energy carrier and fuel cell as a system. Though Sir William Grove first introduced the concept of a fuel cell in 1839 (Grove, 1839), the fuel cell research has emerged as a potential field in recent decades.

A fuel cell is an electrochemical energy conversion device that converts chemical energy of fuel into electrical energy just in a single step. It has lots of advantages compared to the conventional systems that produce electricity. Fuel cells are operated highly efficiently, quietly and

environmentally friendly. They are also compact and flexible in size for different purposes as they can act as ideal power generators.

Fuel cells can generate power from a fraction of watt to hundreds of kilowatts. So they may be used in almost every application where local electricity generation is needed. Fuel cell applications may be classified as being either mobile or stationary applications. They are powering buses, boats, trains, planes, scooters, forklifts, even bicycles as mobile applications. The primary stationary application of fuel cell technology is for the combined generation of electricity and heat, for buildings, industrial facilities or stand-by generators. Although development and demonstrations of fuel cells in automobiles usually draw more attention, applications for stationary power generation offer even greater market opportunity. The targets of both market sectors are similar: higher efficiency and lower emissions. The system design for both applications is also similar in principle. But they differ from each other by the choice of fuel, power conditioning and heat rejection (Barbir, 2003). There are also some differences in requirements for automotive and stationary fuel cell systems. For example, size and weight requirements are very important in automobile application, but not so significant in stationary applications (Barbir, 2005). Miniature fuel cells for cellular phones, laptop computers and portable electronics are on their way to the market.

A fuel cell consists of two electrodes separated by an electrolyte. With the aid of electrocatalysts, fuel and oxidant are combined to produce electricity which is shown schematically in Figure 1.1. Generally, in fuel cells the fuel is hydrogen and it splits into its ions on the anode side (negatively charged electrode). Oxygen is the usual oxidizing reactant of

the fuel cell. The reduction of the oxygen occurs on the cathode side (positively charged electrode).

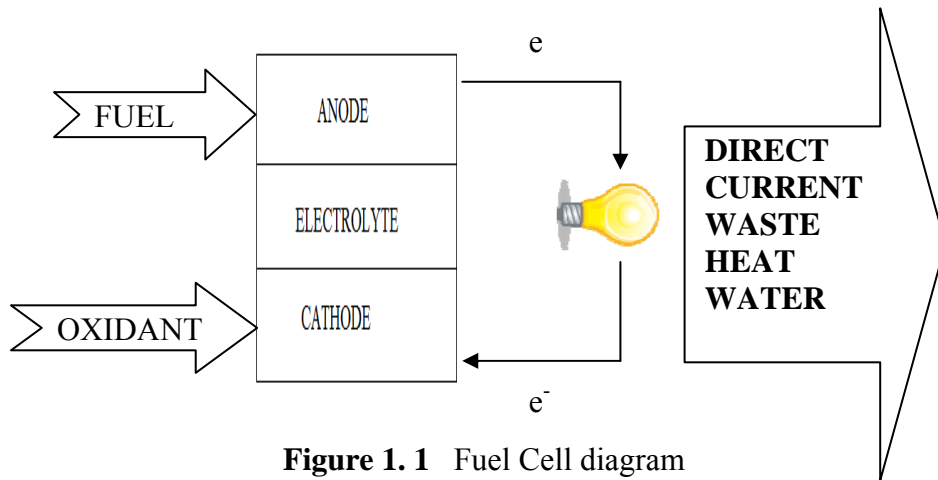


Figure 1. 1 Fuel Cell diagram

The reactant fuel of the cell is stored outside and fed into electrodes only when electricity is required. The capacity is only limited by the size of fuel tanks. When the fuel is exhausted, a fuel cell is similar to an automobile with an empty gasoline tank, being able to be refueled quickly (Li, 2005). A continuous electricity production can be achieved by continuous feeding of the fuel.

Fuel cells are generally categorized by their electrolyte that is the material sandwiched between the two electrodes. The characteristics of this material determine the optimal operating temperature and the fuel used to generate electricity. Each comes with its particular set of benefits and shortcomings. Five types of fuel cells have been under active development, i.e. phosphoric acid fuel cell (PAFC), solid oxide fuel cell

(SOFC), molten carbonate fuel cell (MCFC), alkaline fuel cell (AFC) and proton exchange membrane fuel cell (PEMFC). In addition to the five primary fuel classes, there are two more classes of fuel cells that are not distinguished by their electrolyte. These are the direct methanol fuel cell (DMFC), distinguished by the type of fuel used, and the regenerative fuel cell (RGF) distinguished by its method of operation. The differences of the fuel cell types can be summarized as in Table 1.1. The major differences of the fuel cell types are based on the electrolyte used, the operating temperature, the charge carrier, the requirement of an external reformer, the prime cell components, the catalyst used, and water and heat management.

Table 1.1. Main differences of the fuel cell types

	PEMFC	AFC	PAFC	MCFC	SOFC
Electrolyte	Ion exchange Membranes	Mobilized or immobilized potassium hydroxide	Immobilized liquid phosphoric acid	Immobilized liquid molten carbonate	Ceramic
Operating temperature	80°C	65-220 °C	205 °C	650 °C	600-800 °C
Charge Carrier	H ⁺	OH ⁻	H ⁺	CO ₃ ⁻	O ⁻
Prime Cell components	Carbon based	Carbon based	Graphite based	Stainless based	Ceramic
Catalyst	Pt	Pt	Pt	Ni	Perovskites
Product water management	Evaporative	Evaporative	Evaporative	Gaseous Product	Gaseous Product

Among the types of fuel cells; proton exchange membrane (PEM) fuel cells technology has drawn the most attention because of its simplicity, viability, pollution free operation and quick start up (Barbir, 2005). It is also a serious candidate for automotive applications.

The most commonly used proton exchange membrane is Nafion, which relies on liquid water for humidification of the membrane to transport proton. Nafion possessed inherent chemical, thermal and oxidative stability up to temperatures 80 °C (Zaidi et al, 2009). But it is desirable to increase the fuel cell operation temperature above 100°C. There are several advantages for operating PEMFCs at high temperatures (100-200°C). These advantages are; fast electrode kinetics, simple thermal and water management and heat utilization (Li et al, 2004). Another benefit is the reduced catalyst poisoning by fuel impurities such as CO and CO₂. This poisoning effect has been shown to be very temperature-dependent and it is less pronounced with increasing temperature (Gang et al, 1995). The recent studies are focused on the development of polymer electrolyte membranes for operation at temperatures above 100°C.

High temperature application of a proton exchange membrane fuel cell (PEMFC) can be obtained from polymers with high glass transition temperatures such as polybenzimidazole (Ma, 2004). Among various types of alternative high temperature polymer electrolyte membranes developed so far, phosphoric acid doped polybenzimidazole (poly [2,2-(m-phenylene)-5,5-bibenzimidazole]; PBI) was reported as one of the most promising candidate (Xiao et al, 2005).

PBI is a fully aromatic heterocyclic polymer. It has high chemical resistance and extremely high temperature stability; thus it does not ignite up to 600°C. It holds good mechanical stability in both the dry and hydrated state (Schönberger et al, 2007). It was firstly synthesized by melt polycondensation (Vogel and Marvel, 1961). After that, Iwakura (Iwakura et al, 1964) proposed solution polymerization method for PBI synthesis in which temperature control is easier because of the usage of polyphosphoric acid (PPA) as the reaction solvent and also the lower

reaction temperature (170-200°C). In solution polymerization method firstly; 3,3', 4,4'-tetraaminobiphenyl (3,3'-diamino benzidine) was used as the starting material. But this monomer is quite sensitive to oxidation. Therefore it is more preferable to use 3,3'-diamino benzidine tetrahydrochloride (DAB.4HCl.2H₂O) at which the N-H bonds are closed by HCl to make the monomer defensive against oxidation. The other monomer of the polymerization reaction is isophthalic acid (IPA) and PPA is used as reaction medium.

PBI membranes can be prepared with N,N-dimethylacetamide (DMAc) by solvent casting method. High molecular weight PBI polymers are difficult or incompletely soluble in DMAc. Addition of a minor amount of LiCl (1-5 wt %) in PBI/DMAc is essential as a stabilizer. The concentration of the solution varies between 5 and 20wt%. Below 5wt%, the collapse of polymer chains of PBI is not sufficient to form compact and complex helical structures for membrane formation, which causes subsequent contraction and expansion in the membrane; and above 20wt%, it becomes impossible to obtain a homogeneous solution (Shogbon et al, 2006).

The proton conductivity of pure PBI is low. But after it has been doped by some acids, remarkable high proton conductivity can be achieved even in an anhydrous state (Schuster et al, 2004). PBI can be doped with sulphuric acid, phosphoric acid, perchloric acid, nitric acid and hydrochloric acid (Xing et al, 1999). Phosphoric acid, which can form 3-D hydrogen bonding network due to its special structure, is the most promising one (Ma et al, 2004). It has high boiling point and high thermal stability which acts as a very good proton conductive medium (Kongstein et al, 2007). Phosphoric acid doped PBI membranes can also be operated without humidification of reactant gases.

Phosphoric acid doped PBI membranes were firstly used as polymer electrolyte membranes by Wainright et al (1995). Afterwards, an extensive research has been performed to develop these membranes as PEMs. For the acid doped PBI membranes, high doping levels give high conductivity. But their mechanical stability decreases with increasing doping level, especially at high temperatures (Li et al, 2004). Therefore it is important to select the ideal doping level.

The commercially unavailability of PBI for fuel cell applications made it necessary to synthesize the polymer in laboratory. Yurdakul (2007) developed a synthesis route in which the polymerization starts at 170°C and continues at 200°C. He could obtain the polymer as powders with high molecular weights. According to the results of the measurements of ionic conductivity, it was indicated that the PBI was a promising alternate for the PEMFC operation even at dry conditions.

In general, higher molecular weight of a polymer gives better mechanical strength of the membrane, but it is a critical parameter which should be at the ideal value. Therefore in the present work, PBI polymers with different molecular weights were synthesized by changing the synthesis conditions such as the reaction time (18-24h) and temperature (185°C or 200°C). The polymer was obtained as fibers and characterized by Fourier Transform Infrared Spectroscopy (FTIR), Proton- Nuclear Magnetic Resonance (H-NMR) spectroscopy and elemental analysis. The thermal and mechanical stabilities of PBI and acid doped PBI membrane have been studied by thermogravimetric and mechanical analysis respectively. Acid doped PBI membrane and the pristine membrane was also characterized by X-Ray Diffraction (XRD) analysis. The surface morphology of the PBI based electrodes were examined by Scanning Electron Microscopy (SEM). The performance of the PBI membranes

were tested in a single cell and parameters such as binder of the catalyst, membrane thickness etc, that affects the performance were observed.

CHAPTER 2

PROTON EXCHANGE MEMBRANE FUEL CELLS

Proton exchange membrane fuel cells (PEMFCs) are also known as ion exchange membrane fuel cells (IEMFCs), solid polymer (electrolyte) fuel cells (SP(E)FCs), polymer electrolyte (membrane) fuel cells (PE(M)FCs), etc (Li et al, 2006). More universities and institutes all over the world are becoming involved to the research and development studies of PEMFCs as these fuel cells have become the most promising candidates among the other types. So far several key innovations, such as low platinum catalyst loading, novel membranes, and new bipolar plates, make the application of PEMFC systems more or less applicable.

2.1. Principles of Proton Exchange Membrane Fuel Cells

The proton exchange membrane – also known as polymer electrolyte membrane (PEM) – fuel cell uses a polymeric electrolyte. The proton conducting polymer forms the heart of each cell. Electrodes, usually made of porous carbon with catalytic platinum incorporated into them, are bonded to either side of the electrolyte to form a one-piece membrane–electrode assembly (MEA) (Kuang et al, 2007).

The conversion of chemical energy to electrical energy in a PEM fuel cell occurs through a direct electrochemical reaction. It takes place silently without combustion. To function, the membrane must conduct hydrogen ions (protons) and separate either gas to pass to the other side

of the cell (Zhang et al, 2008). A schematic representation of a PEM fuel cell is shown in Figure 2. 1 (<http://www.udomi.de/fuelcell/fuelcell-basics.html> last accessed at 27.07.2009)

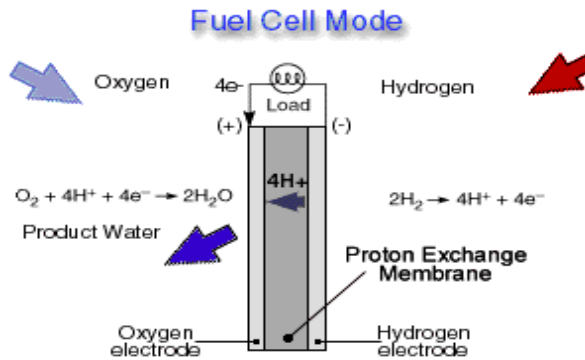


Figure 2. 1 Diagram of PEM fuel cell principle

Unlike in a conventional battery, the fuel and oxidant are supplied to the device from external sources. The device can thus be operated until the fuel (or oxidant) supply is exhausted. As seen in Figure 2. 1, on one side of the cell, hydrogen is delivered through the flow field channel of the anode plate to the anode. On the other side of the cell, oxygen from the air is delivered through the channeled plate to the cathode. At the anode, hydrogen is decomposed into positively charged protons and negatively charged electrons. Positively charged protons pass through the polymer electrolyte membrane (PEM) to the cathode, whereas the negatively charged electrons travel along an external circuit to the cathode, creating an electrical current. At the cathode, the electrons recombine with the protons, and together with the oxygen molecules, form pure water as the only reaction byproduct, which flows out of the cell.

The splitting of the hydrogen molecule is relatively easy using a platinum catalyst. However, the splitting of the stronger oxygen molecule is more difficult, which causes significant activation loss. So far platinum is still the best option for the oxygen reduction reaction (ORR). Another significant source of performance loss is the resistance of the membrane to proton flow, which is minimized by making it as thin as possible (around 50 μm). Nevertheless, the PEM fuel cell is a system whose successful operation with a high power output depends on all the sub-systems; its performance depends on components such as flow field design, catalyst, and membrane, and also on operating parameters such as temperature and humidity (Zhang et al, 2008).

2.2. Main Components of Proton Exchange Membrane Fuel Cells

The main components of a PEMFC are as follows: (1) the ion exchange membrane; (2) the porous electrodes, which is composed of active catalyst layer (the side facing the membrane) and gas diffusion layer (GDL) (3) gaskets for gas tight seal and electrical insulation; (4) bipolar plates that delivers the fuel and oxidant to the reactive sites on both sides. The schematical representation of the PEMFC components is shown in Figure 2.2 <http://www.energi.kemi.dtu.dk/Projekter/fuelcells.aspx> (last accessed at 29.06.2009)

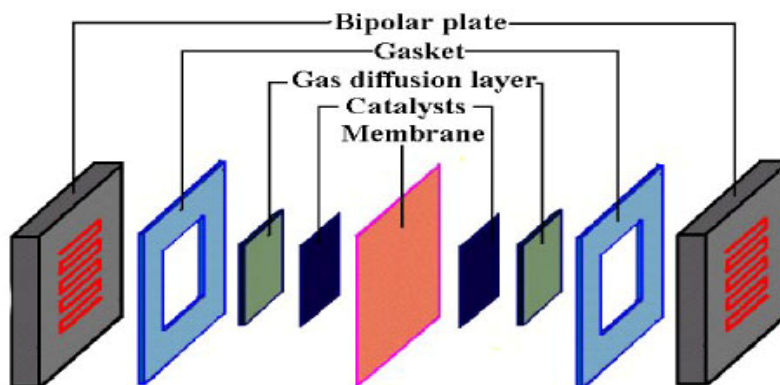


Figure 2.2 Main components of PEMFC

2.2.1. Electrolyte: Membrane

Polymer membrane electrolytes usually consist of a polymer network. Functional groups that are typically acids such as sulfonic acid, are attached onto this polymer network for ion exchange, thus membranes are proton conducting (Li, 2005). In this sense the main function of the membrane in PEM fuel cells is to transport protons from the anode to the cathode. The other functions include keeping the fuel and oxidant separated, which prevents mixing of the two gases and withstanding harsh conditions, including active catalysts, high temperatures or temperature fluctuations, strong oxidants, and reactive radicals. Thus, the ideal polymer must have excellent proton conductivity, chemical and thermal stability, strength, flexibility, low gas permeability, low water drag, fast kinetics for electrode reactions, low cost, and good availability (Panchenko, 2004).

Different types of membranes have been tested for use in PEM fuel cells. The membranes are usually polymers modified to include ions, such as sulfonic groups. These hydrophilic ionic moieties are the key for allowing proton transport across the membrane. The favored polymer

structure has changed to improve membrane lifetime and slow down membrane degradation (Kadirov et al, 2005).

Generally, the life of the PEMFC is determined by the lifetime of the PEM. Thinner membranes increase performance efficiency and proton conductivity. But from the lifetime point of view; they have lower physical strength and higher gas permeability, allowing more gas crossover, which accelerates degradation (LaConti et al, 2003).

One of the most widely used membranes today is Nafion, a polymer created by the DuPont company. Other commercial membranes are Flemion (Asahi Glass), Aciplex (Asahi Chemical), “C” membrane (Chlorine Engineers), and Dow membrane (Dow Chemical) (Barbir, 2005). Nafion has an aliphatic perfluorinated backbone with ether-linked side chains ending in sulfonate cation exchange sites (LaConti et al, 2003). It is a copolymer of tetrafluoroethylene and sulfonyl fluoride vinyl. When the membrane absorbs water, the ionic domains swell and form proton-conducting channels above a critical water content. The conductivity increases with the water content up to a point. Nafion 112 was reported to reach 10000 hours of operation (43–82 °C) (LaConti et al, 2003).

Nafion has limited operation at temperatures up to 80°C since it functions only under highly hydrated state. So different approaches have been studied by research groups for the development of alternate membranes for PEM fuel cells. Sulfonated polyethersulphone (PES) or polyetheretherketone (SPEEK) (Akay, 2008; Erdener, 2007), sulfonated polysulfone/titanium dioxide composite membranes (Devrim, 2009) and phosphoric acid doped polybenzimidazole membranes (Li, 2005) are the new focuses of the field.

2.2.2. Electrodes and Gas Diffusion Layers

A fuel cell electrode is the catalyst layer located between the membrane and gas diffusion layer (GDL). Electrochemical reactions take place on the catalyst surface in the presence of protons, electrons and gases. The catalyst is in contact with ionomer to facilitate the travel of protons through ionomer. Electrons travel through electrically conductive solids including the catalyst which is electrically connected to the GDL. In the reaction sites voids are present too and the reactant gases travel only through these voids. More precisely the electrodes are porous to allow gases to travel to the reaction sites (Barbir, 2005).

Platinum has been considered to be the best catalyst for both the anode and the cathode. The platinum catalyst is usually formed into small particles. Carbon powder that has larger particles, acts as a supporter for them. A widely used carbon-based powder is Vulcan XC72® (by Cabot). This way the platinum is highly divided and spread out, so that a very high proportion of the surface area will be in contact with the reactant, resulting in a great reduction of the catalyst loading with an increase in power (Zhang et al, 2008).

Many researches are focused on developing new platinum based electrocatalysts with high catalytic activity. Platinum and platinum-ruthenium based catalysts on different carbon supports have been prepared by supercritical carbon dioxide deposition and microwave irradiation methods in Bayrakçeken's study. It was observed that the power losses arising from carbon dioxide in hydrogen feed can be decreased by using platinum-ruthenium based catalysts (Bayrakçeken, 2008). Metalphthalocyanines' electrocatalytic activity was also

observed as alternative for oxygen reduction since their highly conjugated structure and high chemical stability (Erkan, 2005).

The catalyst layer typically contains a considerable fraction of ionomer (up to ~30% by weight) to promote ionic transport to/from the main electrolyte membrane (Mench et al, 2008). Several methods were developed for preparation of MEA such as GDL Spraying, Membrane Spraying, and Decal methods (Şengül, 2007).

GDLs are critical components in PEMFCs. The main function of the GDL is to diffuse the gas. The porous nature of the backing material facilitates the effective diffusion of each reactant gas to the catalyst on the MEA. The GDL is also an electrical connection between the carbon-supported catalyst and the bipolar plate or other current collectors. In addition, the GDL also helps in managing water in the fuel cell as it carries the product water away from the electrolyte surface (Zhang et al, 2008).

Firstly GDL is treated with a hydrophobic polymer such as polytetrafluoroethylene (PTFE). PTFE facilitates: (1) gases contact to the catalyst sites by preventing water from “pooling” within the pore volume of the backing layer, (2) the product water to be removed from the cathode and (3) the humidification of the membrane by allowing appropriate amount of water vapour to pass through the GDL and reach the MEA (Li, 2005).

Additionally; GDL provides mechanical support to the MEA by preventing it from sagging into the flow field channels (Barbir, 2005). It is also an elastic component of the MEA to handle the compression needed to establish an intimate contact (Williams et al, 2004).

2.2.3. Bipolar plates

The two plates on each sides of the MEA are called ‘end plates’ or ‘flow field plates’. The fully functioning bipolar plates are essential for multicell configurations, by electrically connecting the anode and cathode of the adjacent cell (Barbir, 2005).

The bipolar plate is a multi-functional component. Its primary function is to supply reactant gases to the gas diffusion electrodes (GDEs) via flow channels. Bipolar plates must provide electrical connections between the individual cells. They have to remove the water produced at the cathode effectively (Davies et al, 2000).

The most common material used for bipolar plates in PEMFC stacks is graphite. Graphite has good electronic conductivity, corrosion resistance and also low density. Composite materials and metals such as steel, copper etc. can also be used as bipolar plates.

2.2.4. Gaskets

Gaskets are placed between MEAs and graphite plates to prevent gas leakage and also the direct contact between acidic electrolyte and the bipolar plate. They also prevent the electrical contact between plates in fuel cell stack systems. The pressure required to prevent the leak between the layers depends on the gasket material and design (Barbir, 2005). Various materials are used for fuel cell. PEMFC operating at typically 80°C has a much wider choice of these materials. The commonly used seal materials are silicone, Teflon and other thermal plastics (Li, 2005). A promising candidate for high temperature operation (100-150°C) of a

PEMFC is viton sheet gasket. It provides excellent heat resistance, offers superior resistance to many chemicals such as acids and also fuels.

2.3. Operation of PEM Fuel Cell

Material properties, cell design and structure, and operating conditions have important effects on the cell power output. Operating conditions include the gas flow, pressure regulation, heat, and water management. High performance of a PEM fuel cell requires maintaining optimal temperature, membrane hydration, and partial pressure of the reactants (Zhang et al, 2008).

2.3.1. Fuel Cell Electrochemistry and Polarization Curve

The overall fuel cell reaction Eq. (2.1) is exactly same as the reaction of hydrogen combustion. Combustion is an exothermic process, which means that there is energy released in the process:



The heat (or enthalpy) of a chemical reaction is the difference between the heats of formation of products and reactants:

$$\Delta H = h_{f, \text{H}_2\text{O}(\text{l})} - h_{f, \text{H}_2(\text{g})} - \frac{1}{2} h_{f, \text{O}_2(\text{g})} = -286 \text{ kJ/mol} \quad (2.2)$$

There are some irreversible losses in energy conversion due to creation of entropy. The portion of the reaction enthalpy that can be converted to electricity corresponds to Gibbs free energy, ΔG , as shown below.

$$\Delta G = \Delta H - T\Delta S \quad (2.3)$$

The values of ΔG , ΔH and ΔS at 25°C are given in Table 2.1 (Weast et al, 1988)

Table 2.1. Enthalpies, entropies and Gibbs free energy for hydrogen oxidation process (at 25°C)

	$\Delta H(\text{kJmol}^{-1})$	$\Delta S(\text{kJmol}^{-1} \text{K}^{-1})$	$\Delta G(\text{kJmol}^{-1})$
$\text{H}_2 + \frac{1}{2} \text{O}_2 \rightarrow \text{H}_2\text{O} (\text{l})$	-286.02	-0.1633	-237.34
$\text{H}_2 + \frac{1}{2} \text{O}_2 \rightarrow \text{H}_2\text{O} (\text{g})$	-241.98	-0.0444	-228.74

For a fuel cell, the work is obtained from the transport of electrons across a potential difference. Electrical work (J/mol) is, in general, described by the relation:

$$W = q E \quad (2.4)$$

where E is the cell voltage and q is the charge (coloumbs/mol). Total charge transferred in fuel cell reaction per mole of hydrogen consumed (q) is expressed as Eq. 2.5

$$q = n N_{\text{avg}} q_{\text{el}} = n F \quad (2.5)$$

where; n is the number of electrons transferred that is equal to 2 for hydrogen fuel cells, N_{avg} is the Avagadro number (6.02×10^{23}), q_{el} is the charge of an electron (1.602×10^{-19} coloumbs/electron) and F is the Faraday's constant (96485 coloumbs/mol.electron).

So the electrical work can be calculated as (Eq.2.6):

$$W = n F E \quad (2.6)$$

The work is represented by the Gibbs free energy due to the electrochemical reaction:

$$W = -\Delta G \quad (2.7)$$

So the cell voltage of the system can be calculated as (Eq. 2.8) when pure hydrogen and oxygen gases were fed at standard conditions

$$E = -\frac{\Delta G}{nF} = \frac{237.34 \text{ (kJ/mol)}}{2 \text{ (electron)} \times 96485 \text{ (C/mol electron)}} = 1.23 \text{ V} \quad (2.8)$$

According to Eq. 2.3 ΔH and ΔS depend on temperature. In case, ΔG depends on temperature too, and consequently the theoretical cell voltage depends on temperature. Table 2.2 shows the theoretical fuel cell potential decreases with temperature, and at typical fuel cell operating temperatures.

Table 2.2. Enthalpy, Gibbs free energy and entropy of hydrogen/oxygen fuel cell reaction with temperature and resulting theoretical potential (Barbir, 2005)

T (K)	$\Delta H(\text{kJ mol}^{-1})$	$\Delta G(\text{kJ mol}^{-1})$	$\Delta S(\text{kJ mol}^{-1} \text{K}^{-1})$	E (V)
298.15	-286.02	-237.34	-0.1633	1.23
333.15	-284.85	-231.63	-0.1598	1.2
353.15	-284.18	-228.42	-0.1579	1.18
373.15	-283.52	-225.24	-0.1562	1.16
423.15	-281.82	-217.14	-0.1491	1.12

The efficiency of any energy conversion device is defined as the ratio between useful energy output and energy input. In case of a fuel cell, the useful energy output is the electrical energy produced, and energy input is hydrogen's higher heating value. Assuming that all of the Gibbs free energy can be converted into electrical energy, the maximum possible (theoretical) efficiency of a fuel cell is (Kakaç et al, 2007):

$$\eta = \Delta G/\Delta H = 237.34/286.02 = 83\% \quad (2.9)$$

Very often, hydrogen's lower heating value is used to express the fuel cell efficiency. In that case the maximum theoretical fuel cell efficiency would be:

$$\eta = \Delta G/\Delta H_{LHV} = 228.74/241.98 = 94.5\% \quad (2.10)$$

The actual fuel cell potential (V_{cell}), and the actual efficiency are lower than the theoretical ones due to various losses (ΔV_{loss}) associated with kinetics and dynamics of the processes, reactants and the products. The actual fuel cell potential is defined as it is shown in Eq. 2.11 where E is the reversible open circuit voltage (OCV):

$$V_{cell} = E - \Delta V_{loss} \quad (2.11)$$

For the actual operation of a PEM fuel cell the potential is decreased from its ideal value because of several irreversible losses. These losses are referred to as;

- (i) Activation- related losses (ΔV_{act})
- (ii) Ohmic losses and (ΔV_{ohm})
- (iii) Mass transport related losses (ΔV_{conc})

Cell voltage can be interpreted in terms of these losses such as:

$$V_{\text{cell}} = E - (\Delta V_{\text{act}} + \Delta V_{\text{ohm}} + \Delta V_{\text{conc}}) \quad (2.12)$$

Firstly some voltage difference is needed to get the electrochemical reactions going. This is called *activation polarization*. Its effect is seen at low current densities. These losses depends on reactions, electrocatalyst material and reactant activities. ΔV_{act} can be written according to the Butler-Volmer Equation 2.13,

$$\Delta V_{\text{act}} = \frac{RT}{\alpha F} \ln \left(\frac{i}{i_0} \right) \quad (2.13)$$

where R is the gas constant, T is temperature, α is transfer coefficient, i is current density and i_0 is exchange current density.

Activation losses can also be defined as Tafel Equation:

$$\Delta V_{\text{act}} = a + b \log(i) \quad (2.14)$$

$$a = -2.3 \frac{RT}{\alpha F} \log(i_0) \quad \text{and} \quad b = 2.3 \frac{RT}{\alpha F} \quad (2.15)$$

Term b is called the Tafel slope.

At intermediate current densities the cell potential drops linearly with current as a result of ohmic losses. These losses are caused by ionic resistance in electrolyte, electronic resistance in electrodes and also in other electrically conductive fuel cell components . So it is clear that

these losses depend on material selection. ΔV_{ohm} can be expressed by Ohm's law Equation 2.16

$$\Delta V_{\text{ohm}} = i R_c \quad (2.16)$$

where R_c is the total internal resistance.

The mass transport related losses are a result of mass transfer limitation rates of the reactants and depend on the current density, reactant activity and electrode structure. ΔV_{conc} can be written according to the Nernst Equation.

$$\Delta V_{\text{conc}} = \frac{RT}{nF} \ln \left(\frac{i_L}{i_L - i} \right) \quad (2.17)$$

where i_L is the limiting current density.

Then equation 2.11 is rewritten as equation 2.18

$$V_{\text{cell}} = E - \frac{RT}{\alpha F} \ln \left(\frac{i}{i_0} \right) - i R_c - \frac{RT}{nF} \ln \left(\frac{i_L}{i_L - i} \right) \quad (2.18)$$

Additionally to the mentioned dominant losses there is also crossover losses which can be significant for low temperature fuel cells. Although the electrolyte is practically impermeable to reactant gases, some small amount of hydrogen can diffuse from anode to the cathode. But the rate of hydrogen permeation is several orders of magnitude lower than hydrogen consumption rate. So these losses may appear insignificant in fuel cell operation. However at open circuit voltage (OCV) these losses may have an effect on cell potential due to the high concentration of

hydrogen on the membrane surface. So it may lead to a drop on OCV (Barbir, 2005).

The polarization curve; which represents the cell voltage-current relationship (Figure 2.3), is the standard figure of fuel cell performance that also represents the losses .

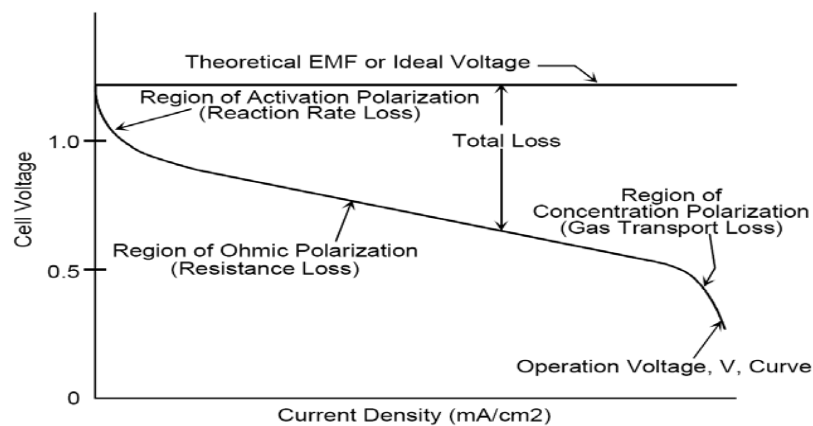


Figure 2. 3 Typical polarization curve for fuel cell with significant losses (Barbir, 2005)

2.3.2. Effect of Temperature on Theoretical Cell Potential

The cell temperature is an operating parameter that plays an important role in the cell operation. The fuel cell reaction is exothermic; therefore it generates heat as a by-product. To maintain the desired temperature, heat must be removed from the system. Some heat dissipates from the outer surface of the fuel cell and the rest must be taken away with a cooling system (Kakaç et al, 2007).

The theoretical cell potential changes with temperature by combining Eq 2.3 and Eq. 2.8 that yields to 2.20:

$$E = - \left(\frac{\Delta H}{nF} - \frac{T\Delta S}{nF} \right) \quad (2.19)$$

According to Eq. 2.19 and seen in Table 2.2 an increase in the cell temperature results in a lower theoretical cell potential (Barbir, 2005) .

2.3.3. High Temperature Operation of PEMFC

There are several technological and commercial reasons for operating PEM fuel cells at temperatures above 100°C. They can be listed as seen below:

- (1) All the reaction kinetics and the catalytic activity are enhanced for both electrode reactions.
- (2) High temperature operation of PEMFC involves gas phase of water, however at lower temperatures it involves gas and liquid phase.
- (3) The poisoning effect of the catalyst by fuel impurities (such as CO) is reduced (Gang et al, 1995).
- (4) The temperature gradient between the fuel cell stack and the coolant is increased (Zhang et al, 2006).
- (5) Waste heat can be recovered as a practical energy source. It can be used for direct heating, steam reforming or for pressurized operation in the system. In this way the overall system efficiency will be increased.

2.4. High Temperature Proton Exchange Membranes

The most extensive limitations of perfluorinated ionomers (commonly Nafion) arise from the fact that these materials are proton-conducting only when they are hydrated. This property results in a maximum operating temperature of ~ 100 °C that in turn limits activity and CO tolerance of the electro catalyst. Other drawbacks of this type of membrane are the need of permanent humidification, high methanol crossover, and limited mechanical stability (Sukumar et al, 2006).

Accordingly, a variety of alternative approaches using materials that are cheaper and more suitable for higher temperatures have emerged. Based on the classification of proton solvents, there are three basic approaches to high temperature PEMs:

(a) Membranes that use water as proton carrier. Efforts have been made at retaining water in the membrane at higher temperatures.

(b) Anhydrous proton-conducting polymers where the proton is transferred not through water, but through other proton solvents such as phosphate ion (H_4PO_4^+ and H_2PO_4^-) (e.g. polybenzimidazole (PBI)/ H_3PO_4 system) and imidazole (e.g. sPEEK/imidazolesystem) (Ma, 2004).

(c) Membrane where the proton transport involves mixture of two proton solvents, such as water and phosphate ions.

Among various types of alternative high temperature polymer electrolyte membranes developed so far, phosphoric acid doped polybenzimidazole (poly [2,2-(*m*-phenylene)-5,5-benzimidazole]; PBI) was reported as one of the most promising candidate showing high conductivity, good

thermal stability and good fuel cell performance at temperatures up to 200°C and low relative humidity (Xiao et al, 2005)

2.5. General Information about Polybenzimidazoles

Since Vogel and Marvel (1961) synthesized the first aromatic polybenzimidazoles (PBI), a great deal of attention on PBI have received from both academia and industry. PBI can be in the aromatic or aliphatic structure according to the monomers that consists of. In general, aromatic polybenzimidazoles have remarkably better thermal properties than aliphatic ones. However, the thermal properties of the former are reduced if there is an oxygen, siloxane, silane, phosphine oxide, sulfur or sulfone bridge between aromatic units. These bridge units generally enhance polymer solubility and processability (tractability). Because poly (2,2'-(m-phenylene)-5,5' bibenzimidazole) (PBI) offers a combinations of thermal stability and processability, it has received most attention in polybenzimidazole study.

The newer polybenzimidazole membranes (PBI) offer an alternative to Nafion, with different opportunities and challenges in PEM fuel cell applications. They do not rely on liquid water to transport protons through the membrane, but (in most cases) on phosphoric acid doping. Phosphoric-acid doped PBI fuel cells can function at temperatures as high as 200 °C. Not relying on liquid water, PBI cells can operate well beyond 100 °C without any need for pressurisation: this generates a number of very interesting properties, in particular from the point of view of controllability (Zenith et al, 2007).

2.5.1. Synthesis of PBI

PBI is a fully aromatic heterocyclic polymer. It has high chemical resistance and extremely high temperature stability; thus it does not ignite up to 600°C. It holds good mechanical stability in both the dry and hydrated state (Schönberger et al, 2007). It was firstly synthesized by melt polycondensation (Vogel and Marvel, 1961). After that, Iwakura (1964) proposed solution polymerization method for PBI synthesis in which temperature control is easier because of the usage of polyphosphoric acid (PPA) as the reaction solvent and also the lower reaction temperature (170-200°C). The differences in the two polymerization methods are given in Table 2.3 and the reactions are given in Figure 2. 4 and Figure 2.5.

Table 2.3 The differences between the synthesis methods of PBI (Olabisi et al, 1996)**

	Solution Polycondensation	Melt Polymerization
Major Monomers	Diaminobenzidine (DAB) and isophthalic acid (IPA)	Diaminobenzidine (DAB) and diphenyl isophthalate (DPIP)
Reaction Temperature	170-200 °C	1 st stage: 270 °C 2 nd stage: 360 °C
Reaction medium	Nitrogen atmosphere	Nitrogen atmosphere
By products	Water	Phenol and Water
Antifoaming agent	No	Dependent on the process condition
Catalysts	Optional	Optional
Cost	Medium	High

** Some data are updated according to the recent developments

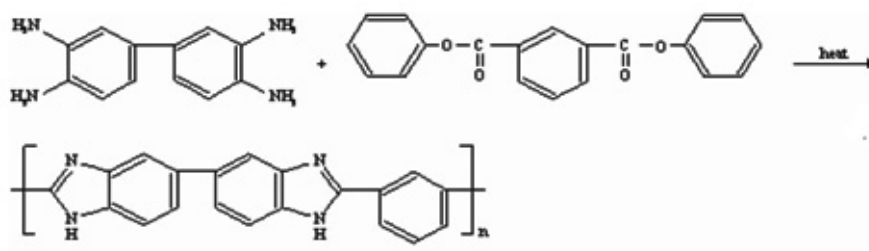


Figure 2. 4 Reaction scheme of PBI by melt polycondensation

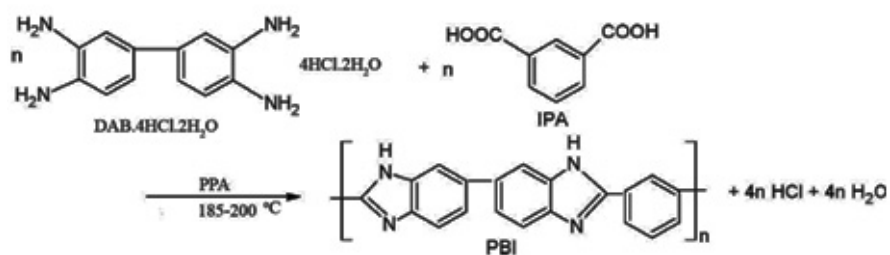


Figure 2. 5 Reaction scheme of PBI by solution polymerization

2.5.2. Phosphoric Acid Doped PBI Membranes and Proton Conduction Mechanism

Phosphoric acid doped PBI or ABPBI (Poly(2,5-benzimidazole)) membranes have generally been prepared by three methods (Weng et al, 1996):

Method 1: Cast from a solution of polymer in NaOH/ethanol solution under nitrogen environment, and washed by water until pH 7, then doped by immersion in phosphoric acid solution. This method was proposed initially for acid doped ABPBI membranes (Ma, 2004).

Method 2: A 3~5 wt% suspension of PBI in N, N-dimethylacetamide (DMAc) with 1~2 wt% LiCl is heated to 80°C and mixed in an ultrasonic bath. Magnetically stirring is also applied to prevent the polymer from aggregating. The obtained solution is cast on a clean glass plate and evaporated in an oven at 80°C for at least four hours. The films are washed by boiling water to remove the LiCl, dried in a vacuum oven, and then doped by immersion in phosphoric acid solution (Yurdakul, 2007). Most of PBI membranes reported in the literature were prepared by the DMAc method (Li et al, 2004; Schuster, 2004).

The final acid loading for method (1) and (2) is calculated from the weight difference of the membranes before and after the immersion.

Method 3: PBI and acid directly cast from a solution of PBI and H₃PO₄ in a suitable solvent such as trifluoroacetic acid (TFA). The solvent is evaporated and the film is ready for use.

The direct casting method from TFA/acid solution is an easy way to prepare acid doped PBI membranes, which have well controlled acid doping level.

Even though the doping levels are similar, the properties of films formed by the various methods are substantially different. Films cast using the DMAc method are normally stronger and tougher than those cast from TFA (Ma , 2004).

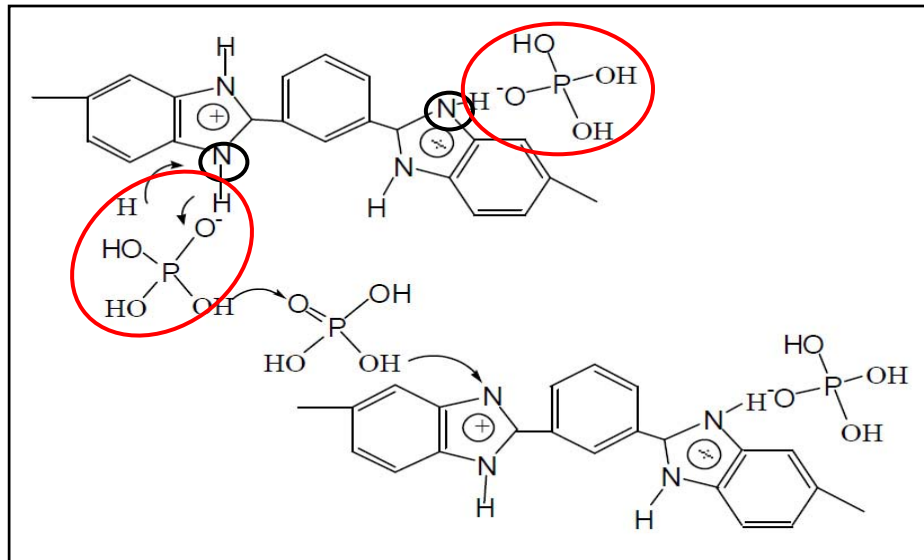
PBI is a basic polymer ($pK_a = 5.23$ as protonated) so it can readily react with a strong acid. The proton conduction of H_3PO_4 doped PBI can be explained with two mechanisms.

In PBI, the nitrogen of the imide group acts as a strong proton acceptor. So the acid doped PBI membranes can have only two molecules H_3PO_4 per PBI repeat unit as bonded acid. The mentioned proton hopping from the N-H site to a H_3PO_4 anion is observed when the doping level of the membrane is less than 2 that is the number of theoretical bonded H_3PO_4 to the imide group of PBI. This mechanism is seen in Figure 2.6.a.

However, the acid doping level that is less than 2 is not sufficient for conductivity. As it is seen in Figure 2.6.b there is a proton hopping along the $H_2PO_4^-$ anionic chain which shows the contribution of free acids to conductivity (Li, 2005).

The proton conductivity of acid-doped PBI is influenced by relative humidity, temperature and doping level. The conductivity of the 11 mole acid doped membrane at $150^\circ C$ and 33% relative humidity was 0.12 S/cm. Moreover, the conductivity value for the same membrane was measured as 0.053 S/cm at $150^\circ C$ in dry air which was a promising level for a high temperature fuel cell operation without humidity (Yurdakul, 2007).

(a)



(b)

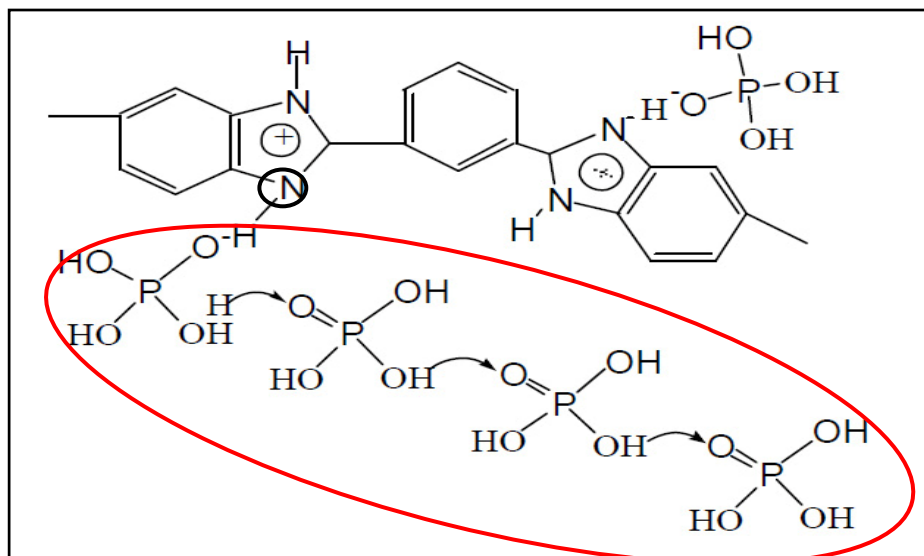


Figure 2. 6 Proton conduction mechanism of H_3PO_4 doped PBI (a) when acid doping level is less than 2 (b) when acid doping level is more than 2.

CHAPTER 3

EXPERIMENTAL

3.1. Preparation of Phosphoric Acid Doped Polybenzimidazole Membranes

3.1.1. Materials

The materials used in this study are required for the synthesis of polybenzimidazole (PBI) and preparation of membrane electrode assemblies. For polymer synthesis; the monomers DAB.4HCl.2H₂O (≥98 %) and isophthalic acid (99%) and the polycondensing agent polyphosphoric acid (115%) were purchased from Sigma Aldrich. CaCl₂ was obtained from Merck to be used as the drying agent during polymerization period. Sodium bicarbonate (Merck) was purchased as the washing chemical of the polymerization reaction solution. 98 wt. % sulphuric acid was obtained from Sigma Aldrich to be used for the determination of molecular weight of the polymer. DMAc (Merck) as the membrane solution solvent, LiCl (Merck) as the stabilizer agent of the membrane solution and 85% o- phosphoric acid (extra pure, Merck) used for acid doping were bought. The distilled water was obtained from tap water by using water distillation apparatus (Nüve NS 108).

For the catalyst ink preparation 20 wt. % Pt on carbon (E-tek) was used as the catalyst and polyvinylidene fluoride (PVDF) (Sigma Aldrich) as the

binder. Gas diffusion layer was purchased from Sigracet® GDL 31 BC (SGL Carbon).

Gases used were nitrogen (99.999% pure), hydrogen and oxygen (99.9999% pure) from Linde (Turkey).

3.1.2. Polybenzimidazole Synthesis

In this work PBI polymers were synthesized by Solution Polymerization method (Iwakura et al, 1964) that is explained in Section 2.5.1. The monomers were diamino benzidine tetrahydrochloride (DAB.4HCl.2H₂O) and isophthalic acid (IPA). The reaction solvent was polyphosphoric acid (PPA). The polymerization occurs in nitrogen atmosphere at 185-200°C for 18-24 hours. The polymerization reaction is shown in Figure 3. 1.

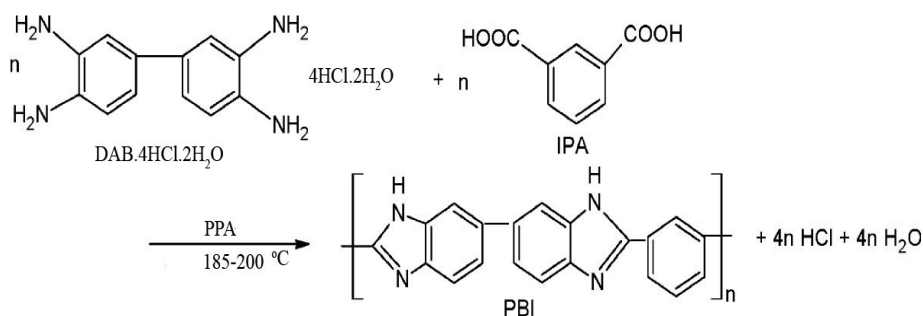


Figure 3. 1 Reaction scheme of PBI synthesis with solution polymerization method

For the synthesis of PBI; the reactor was a four necked glass flask equipped with a mechanical stirrer (Heidolph RZR 2041), nitrogen inlet, thermocouple (Pt 100) and a CaCl₂ drying tube. The reactor was heated

by an electrical heater and the temperature was controlled by a digital temperature controller. The picture of the set-up for experiments is given in Figure 3. 2.

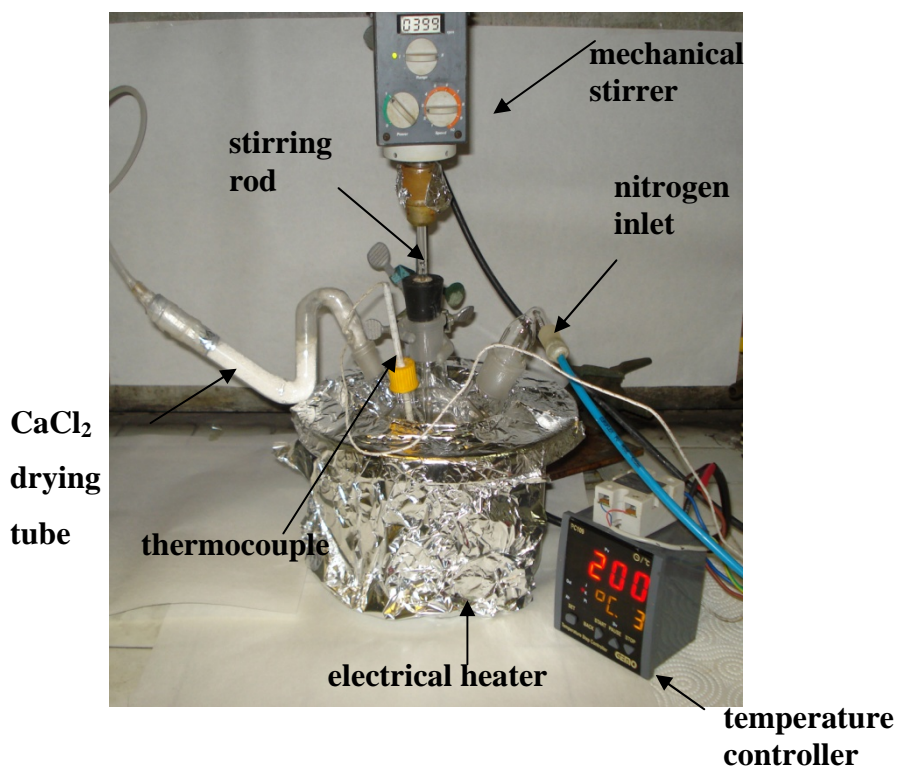


Figure 3. 2 The picture of the experimental set up for PBI synthesis

The experimental procedure is as follows. Firstly a specific amount of PPA was heated to 140 °C. Then the first monomer DAB.4HCl.2H₂O was added. During dissolving DAB.4HCl.2H₂O in PPA, bubbles were formed on the surface of the reaction solution. These bubbles were due to the elimination of HCl gas from DAB. After all bubbles disappeared, about 2 hours later, an equimolar amount of IPA was added into the solution.

The reaction mixture was stirred continuously at 185-200 °C for 18 to 24 hours. As reaction proceeds the viscosity of the mixture was increased progressively and finally the highly viscous polymer solution was obtained. Then this solution was slowly poured into a beaker filled with DI water as shown in Figure 3.3. During pouring, the fiber form of the polymer was seen clearly. The solid polymer was washed with DI water for several times, and the precipitate was treated with 5 wt. % sodium bicarbonate in order to neutralize the polymer. Then, the polymer fiber was washed with DI water several times until the pH of the washing water was neutral. It must be emphasized that this purification step is very important for the solubility of the polymer in membrane solution. Finally; the polymer was left into the oven at 150°C for drying. The schematic representation of the purification procedure is shown in Figure 3.3.



Figure 3.3 The picture of the purification procedure

3.1.3. Membrane Preparation

PBI membranes were prepared by the solution casting method which was previously explained in Section 2.5.2 as Method 2. PBI polymer (Figure 3.4.a) was solved in N,N dimethylacetamide (DMAc) and lithium chloride and 2.5 wt. % and 5 wt. % PBI solutions were obtained. 1.5-3.0 wt. % of LiCl was used as the stabilizer. The solution was mixed in an ultrasonic bath at 80°C and also magnetically stirred (Figure 3.4.b). The homogeneous solution was cast onto Petri dishes. The thickness and the size of the membranes were varied by controlling the volume of the solution. After casting, DMAc was evaporated in a ventilated oven in a temperature range from 80 to 120°C for 24 hours. Followingly; the prepared membranes were immersed into boiling deionized water for 5 hours to remove LiCl. A final drying is applied at 190°C to remove the traces of the solvent. The picture of the prepared membrane is shown in Figure 3. 4.c.

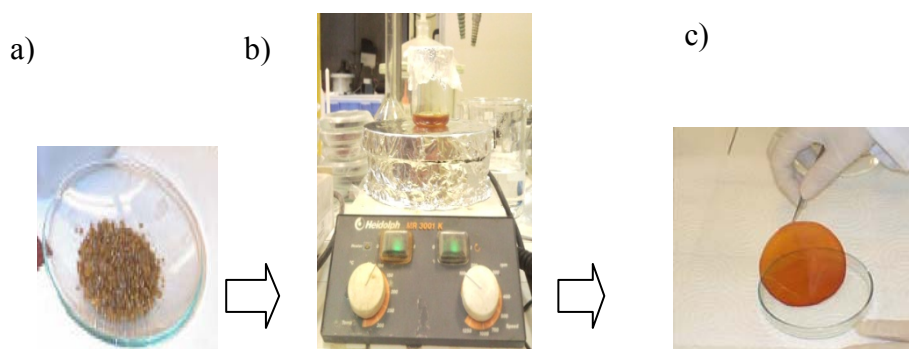


Figure 3. 4 PBI membrane preparation a) PBI powder b)Membrane Solution c)PBI membrane

3.1.4. Acid Doping of the Membranes

The PBI membranes were immersed into phosphoric acid having different concentrations (75-85%) in order to achieve proton conductivity. In order to reach a total saturation, they were left at least 2 weeks in the acid. The amount of phosphoric acid attached to PBI in each case was dependent on the molecular weight of PBI and immersion time in acid. The doping level was estimated by the weight increase of the sample before and after doping:

$$\text{Acid doping} = \frac{\text{weight difference}}{\text{initial weight}} \times \frac{\text{Mw of PBI repeat unit}}{\text{Mw of H}_3\text{PO}_4} \quad (3.1)$$

A sample calculation of acid doping level and the time vs doping level plot are given in Appendix A.

3.2. Characterization of Polybenzimidazole Polymer

The chemical structure of the synthesized polymer was characterized by Proton Nuclear Magnetic Resonance Spectra, $^1\text{H-NMR}$; Fourier Transform Infrared Spectroscopy, FTIR; and elemental analysis. The synthesis conditions of the polymerization that includes reaction temperature and time were changed and their effects on molecular weight were examined.

3.2.1 Nuclear Magnetic Resonance Spectra

The nuclear magnetic resonance (NMR) spectra of PBI were determined by the analysis of $^1\text{H-NMR}$ using a 300 MHz spectrometer (Bruker). The

PBI sample was dissolved in DMSO- d_6 (concentration: 6mg sample/1 ml). The spectrum range was 1-15 ppm.

3.2.2. Fourier Transform Infrared Spectroscopy

The chemical structure of the synthesized polymer was determined by Fourier Transform Infrared Spectroscopy (Bruker IFS 66/S). For the FTIR spectra, PBI solution in DMAc was placed drop wise onto the KBr tablet. The FTIR spectra were recorded in the 4000–400 cm^{-1} range, with 40 scans at 4 cm^{-1} resolution.

3.2.3. Elemental Analysis

The percentage of the elements in the PBI structure were observed by elemental analysis (LECO, CHNS-932). The carbon (C), hydrogen (H) and nitrogen (N) percentages of a 2 ± 0.0001 mg sample were determined by combustion method at 950-1000°C.

3.2.4. Determination of Molecular Weight

It is well known that Ubbelohde viscometer is a useful instrument of determining the viscosity of polymer solution. In general, to determine the viscosity of polymer solution, a thoroughly cleaned viscometer was used firstly to measure the flow time of the pure solvent namely t_0 . After drying it, the flow time of polymer solution with different concentrations, namely t , was measured secondly. Specific viscosity, η_{sp} , and intrinsic viscosity, $[\eta]$, of polymer solution can be determined by following equations (3.2) and (3.3), by using obtained t and t_0 (Quian, 1958).

$$\eta_{sp} = \frac{t-t_0}{t} \quad (3.2)$$

$$\eta_{red} = \frac{\eta_{sp}}{c} \quad (3.3)$$

$$\eta_{rel} = \frac{t}{t_0} \quad (3.4)$$

$$\eta_{inh} = \frac{\ln(\eta_{rel})}{c} \quad (3.5)$$

$$[\eta] = \lim_{c \rightarrow 0} \frac{\eta_{sp}}{c} \quad (3.6)$$

where c is the concentration of the PBI solution.

The molecular weight of the synthesized PBI polymers were determined by Ubbelohde viscometer method. Four solutions of 0.25, 0.5, 0.75, and 1 g/dl PBI in 98% sulphuric acid were prepared. Flow times of all the solutions and the pure solvent were measured at 30°C in an Ubbelohde viscometer with the system shown in Figure 3. 5. Molecular weight, M_w , was calculated by Mark Houwink equation as follows:

$$[\eta] = K (M_w)^a \quad (3.7)$$

where K and a are constants that depends on the polymer, solvent and temperature. The values are taken from literature: $K = 1.94 \times 10^{-4}$ and $a = 0.791$ (Buckley et al, 1987)

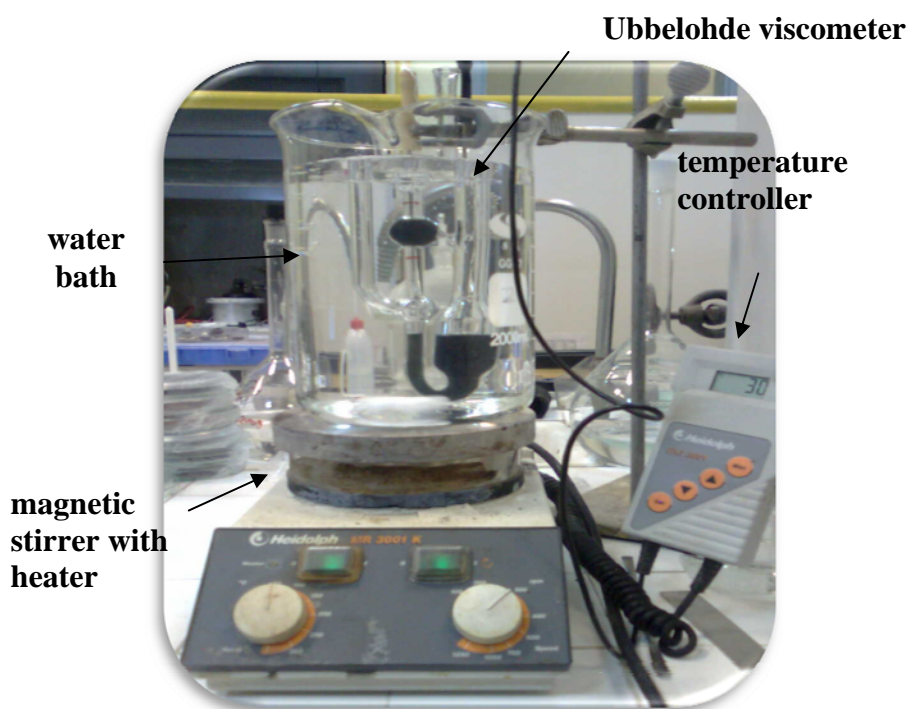


Figure 3. 5. The experimental setup of viscosity measurement

3.3. Characterization of the membranes

3.3.1. Fourier Transform Infrared Spectroscopy

The FTIR spectra of the pristine PBI membranes and also the phosphoric acid doped PBI membranes were determined by the same technique as explained in section 3.2.2.

3.3.2. Thermogravimetric analysis

Thermal stability of the membranes the weight gain due to both water and phosphoric acid were observed by thermogravimetric analysis. For

thermogravimetric (TGA) analysis; undoped and doped PBI membrane samples were heated from 25 to 1000°C at a heating rate 5 °C/min under nitrogen atmosphere (DuPont 2000).

3.3.3. X- Ray Diffraction Analysis

100 kV Philips twin tube X-ray diffractometer (PW/1050, CuK α λ = 1.5406 Å) was used for the XRD analysis of the PBI membranes. The measurements were done in the range of $0^\circ \leq 2\theta \leq 100^\circ$ (X ray; 40 kV / 40 mA). The analysis was performed both on non-doped membranes and on doped membranes.

3.3.4. Mechanical analysis

Mechanical strength of the membranes was measured with a vertical film device (INSTRON 3367). The initial dimensions of the samples were 10 mm in width (wm), 60 μ m in thickness (tm) and 10 mm in length (lm). The experiments were performed with a constant stretching speed of 5 mm/min in ambient air. The samples of PBI membranes with different molecular weights and also different doping levels were examined.

3.4. Preparation of Membrane Electrode Assembly

3.4.1. Membrane Electrode Assembly Preparation Technique

MEAs were prepared by spraying catalyst ink on to the gas diffusion layers (GDL 31 BC, SGL Carbon Germany (Bayrakçeken, 2008)). The general procedure was as follows: firstly the catalyst ink that is

composed of the catalyst, binder and the solvent was prepared. By the time the ink was ready; it was sprayed onto the GDL until reaching a Pt loading of 0.4 mgPt/cm^2 . Then these electrodes were dried in an oven for the removal of the solvent traces. Finally the prepared electrodes were hot pressed onto both sides of the membrane.

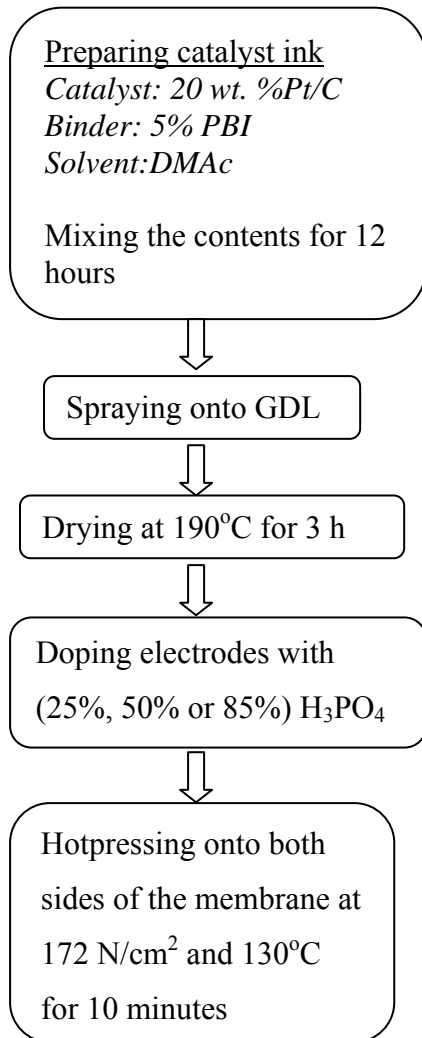
In this study; in the light of the mentioned method; two procedures were applied in which the binder differs in the catalyst ink. The flow charts of both procedures are summarized in Figure 3.6. In both procedures 20wt % Pt/C was used as the catalyst and DMAc as the solvent. As it is seen from the figure, the major difference is the content of the binder.

In the first method; 20 wt% Pt/C (E-Tek Inc.) as the catalyst and 5wt% PBI solution as the binder were mixed in DMAc for 12 hours to prepare the catalyst ink. The ink was sprayed onto the GDLs until the required Pt loading was attained (0.4 mg Pt/cm^2 for both anode and cathode sides). The catalyst loading was controlled by weighing the GDLs at different times. After the catalyst ink was sprayed onto the GDL, the electrodes were left to the oven at 190°C for three hours to remove the solvent traces. Subsequently, the electrodes were impregnated with phosphoric acid (85 %, 50%, 25%) in order to dope the PBI in the catalytic layer and soften the ionic contact. Finally the electrodes were hot pressed onto both sides of the membrane at 130°C (Kongstein et al, 2007) and 172 N/cm^2 for 10 minutes.

In the second procedure; PVDF was used in addition to PBI as the binder in the catalyst ink. PVDF is a semi-crystalline and hydrophobic polymer. There is strong interaction between the $>\text{CF}_2$ groups of PVDF and the N-H groups of PBI. The applied procedure was as follows: For this time 1 wt.% PVDF was used as the binder in addition to 5 wt.% PBI. Firstly the

catalyst ink, that includes the catalyst, binder and the solvent, was prepared by mixing for 12h (Li et al, 2008). After spraying the catalyst on, the electrodes were dried in the oven at 150°C for 1 hour to evaporate the remaining DMAc. The electrodes and the PBI membrane with a doping level of 700-800 mol% phosphoric acid molecules per repeating unit of PBI were pressed at 172 N/cm² and 150°C for 10 minutes.

1st Procedure



2nd Procedure

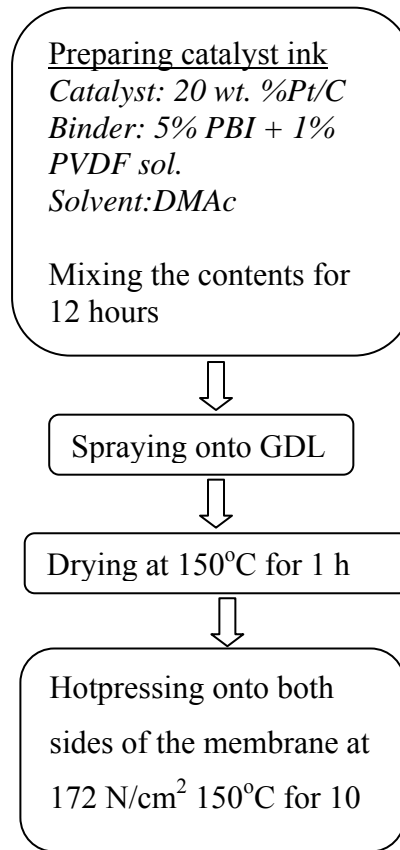


Figure 3. 6 Flow charts of MEA preparation

Detailed information about MEA preparation is given in Appendix B.

3.4.2. Surface Morphology of the Electrodes

The surface morphology of MEA and electrodes were examined in QUANTA 400F Field Emission Scanning Electrode Microscope using both secondary electron (SE) and back-scattered electron (BSE) modes under similar experimental conditions: same current of primary beam, same scan rates, and same pixel resolution. Additionally the distribution of Pt element on the surface of the electrode was analyzed by Energy Dispersive X-ray Spectroscopy (EDX).

3.5. PEMFC Performance Tests

The MEAs with an active area of $2.1 \times 2.1 \text{ cm}^2$ were tested in a fuel cell test station built at METU Fuel Cell Technology Laboratory. A single PEM fuel cell (Electrochem, FC05-01SP-REF) was used in the experiments (Figure 3. 7). The fabricated power of the cell was manipulated by an electronic load (Dynaload_RBL488), which can be controlled either manually or by a computer. The current and voltage of the cell were monitored and logged throughout the operation of the cell by the fuel cell test software (FCPower_ v. 2.1.102 Fideris). The single PEM fuel cell sealing and the compression are very important. If sealing had failed hydrogen and oxygen gases would be mixed and since there is catalyst MEA could burn resulting in the burning of the MEA (Bayrakçeken et al, 2008). Viton gaskets are used to prevent the gas leakage that are also resistant to acid and also high temperature. In order to prevent the condensation, the gas transfer lines between the

humidifiers and the fuel cell were built with electrical-resistive-heaters. That is, the temperatures of the heated gas transfer lines were kept at a set temperature by on/off type temperature controllers (Erkan, 2005). The fabricated MEA was placed in the test cell and the bolts were tightened with a torque of 1.7 Nm on each bolt.

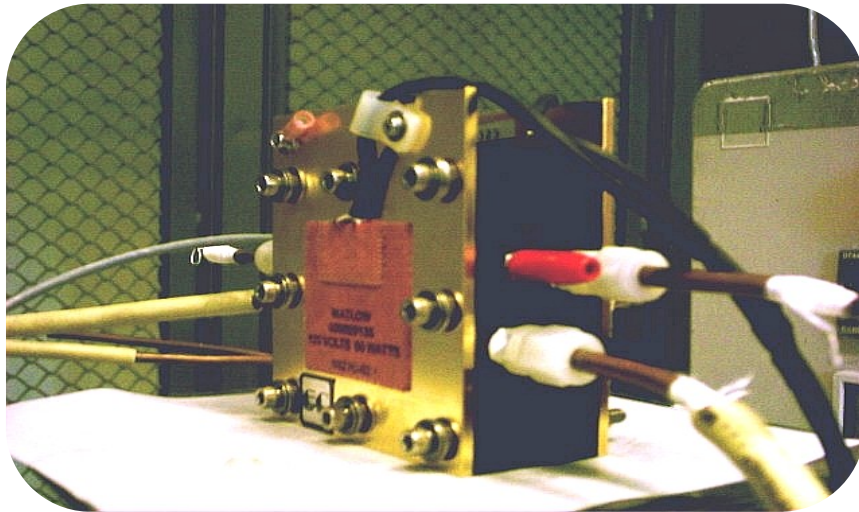


Figure 3. 7 Single PEM fuel cell

In the test station; oxygen and hydrogen was used as oxidant and fuel, respectively. The reactant gases were sent to the fuel cell through Aalborg-171 mass flow controllers at a rate of 0.1 slpm. Prior to entering the fuel cell, the gases were transferred through the stainless steel gas lines and heated with resistance heaters. PID temperature controllers were used to operate the system at a required temperature. The cell was operated at 0.5 V until it came to steady state. After steady state was achieved, starting with the open circuit voltage (OCV) value, the current–voltage data were logged by changing the load.

A schematic representation and a picture of the test station are given in Figure 3.8 and Figure 3.9, respectively. PEM fuel is modified for high temperature operation. The material of the fittings and gas transfer lines were changed to stainless steel to make them resistant to high temperature. The gasket material was chosen as Viton that is not only applicable at high temperatures but also resistant to acid which causes serious deformation on other gasket materials such as silicone. Throughout this study only hydrogen and oxygen gases were fed to the fuel cell system and the performance analysis were done by using dry gases.

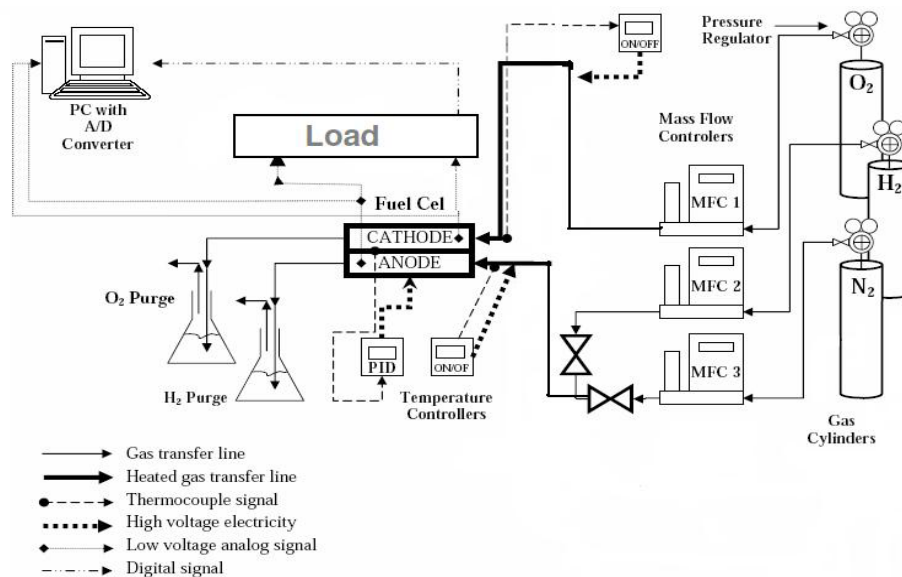


Figure 3. 8 Schematic representation of fuel cell test station (modified version of Erkan, 2005)

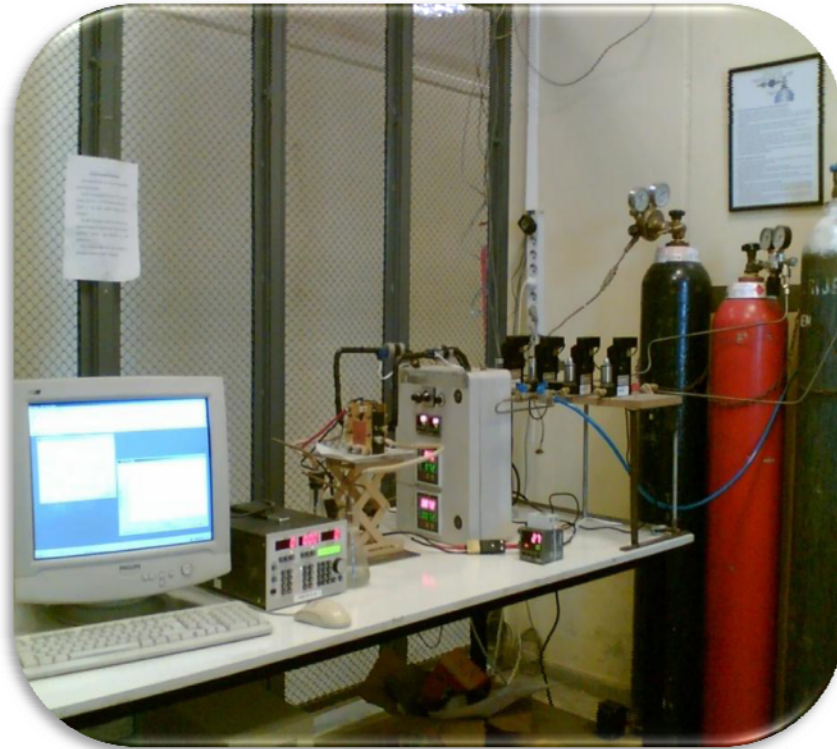


Figure 3. 9 The Picture of the PEM fuel cell test station

3.6. Scope of the Experiments

The flow chart of the performed experiments were summarized in Figure 3.10. As it is seen; the experiments have started with PBI synthesis and followed by membrane preparation, acid doping of the membrane and preparation of PBI based MEAs. Finally the PEM fuel cell performance tests were done in the fuel cell test station which was built in METU Fuel Cell Research Laboratory. It was aimed to observe effects of several parameters on PEMFC performance. The parameters that are studied throughout this study are as follows;

- a) Effect of the binder used in the catalyst ink
 - i) The effect of H_3PO_4 concentration that doped to the electrodes (in 1st procedure of MEA preparation explained in Section 3.4.1)
 - ii) The effect of PVDF:PBI ratio in the catalyst ink (in 2nd procedure of MEA preparation explained in Section 3.4.1)
- b) Effect of operating temperature (125-160°C)
- c) Effect of membrane thickness (70-100 μm)

To observe the effects of these parameters, the following test parameters and conditions were used:

- a) Membranes cast from PBI polymer with an average molecular weight of: 81200
- b) Doping level of the membranes: 700 mol% H_3PO_4 /repeating unit of PBI
- c) Catalyst loading: 0.4 mg Pt/cm² (for both anode and cathode sides)
- d) Flow rates of O_2 and H_2 : 0.1 slpm (without humidification of reactant gases)

Test Conditions of performed experiments for fuel cell performance tests are summarized in Table 3.1.

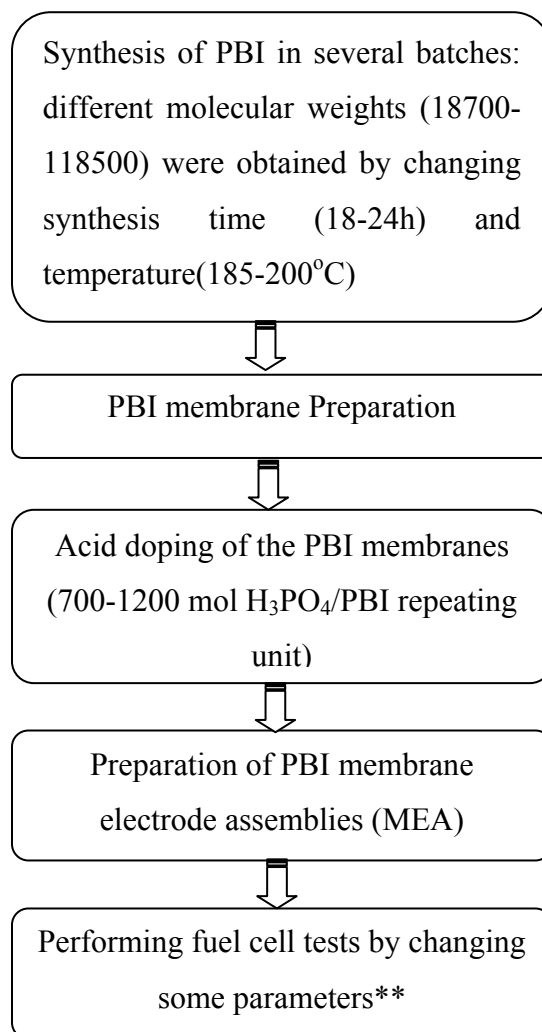


Figure 3. 10 Flow chart of the experiments

****Table 3.1** Test Conditions of performed experiments for fuel cell performance tests

Test Condition	PVDF:PBI ratio in catalyst ink	H ₃ PO ₄ concentration used to dope the electrodes (%)	Temperature (°C)	Thickness (μm)
1	0:1	85	150	80
2	0:1	50	150	80
3	1:3	-	150	80
4	1:1	-	150	80
5	3:1	-	150	80
6	1:3	-	125	80
7	1:3	-	160	80
8	1:3	-	150	70
9	1:3	-	150	100

CHAPTER 4

RESULTS AND DISCUSSION

4.1. Characterization of PBI Polymer

In the present study PBI was synthesized by solution polymerization method. The synthesis was repeated for 20 times. The chemical structure of the synthesized polymer was validated by Proton Nuclear Magnetic Resonance Spectra, H-NMR; Fourier Transform Infrared Spectroscopy, FTIR; and elemental analysis. The synthesis conditions of the polymerization that includes reaction temperature and time were changed and their effects on molecular weight were examined.

4.1.1. Nuclear Magnetic Resonance Spectra

Proton resonances in the NMR spectrum of PBI were studied by H-NMR. PBI exhibits similar behavior in both DMSO-d₆ and DMAC solvents. NMR studies were carried out in DMSO-d₆ solvent, since it is less expensive compared to DMAC (Sannigrahi et al, 2007).

The NMR spectrum of PBI shows many bands due to the molecular environment of the hydrogen atoms present in the structure. Figure 4. 1 shows the H-NMR spectra of PBI with the numbers on peaks belongs to the same numbers as it is shown on the structure. Absorption bands due

to imidazole protons of PBI were observed at 13.3 ppm. The peaks between 7–10 ppm are due to aromatic proton numbers (Kojima et al, 1980).

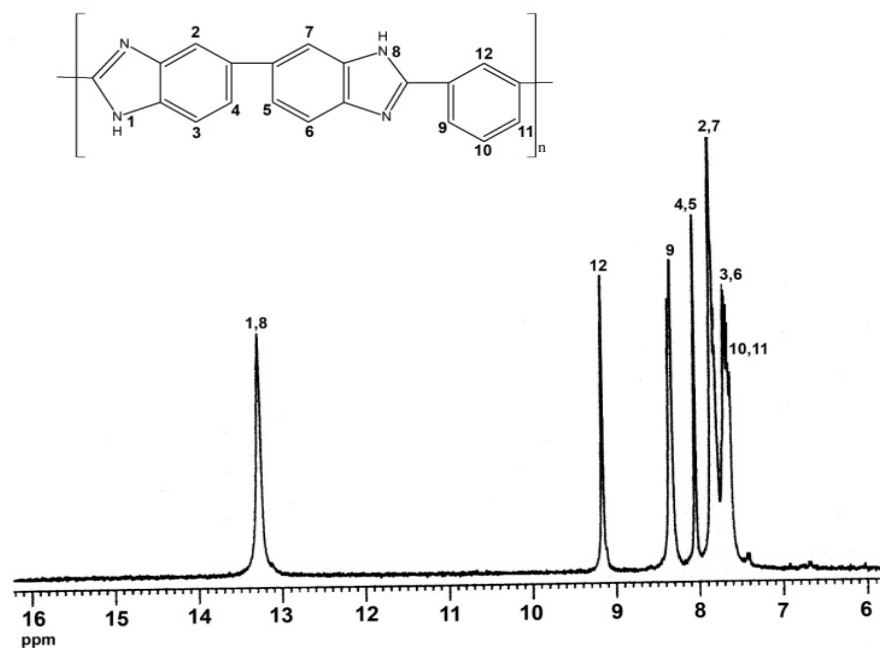


Figure 4. 1. H-NMR spectra of the synthesized PBI

4.1.2. Fourier Transform Infrared Spectroscopy

The main infrared spectral features of PBI were studied by Fourier Transform Infrared Spectroscopy (FTIR). Below 2000 cm^{-1} the spectrum was characterized by some relatively narrow peaks. These peaks were attributed to localized normal vibrations of the phenyl groups in the pristine PBI. The polymer exhibited characteristic absorption bands at 3015 and 1645 cm^{-1} due to the stretching vibration of the N-H groups

and C=N groups respectively as seen in Figure 4. 2 (Chuang et al, 2006). The ‘breathing’ mode of the imidazole ring appears at 1285 cm⁻¹ for PBI.

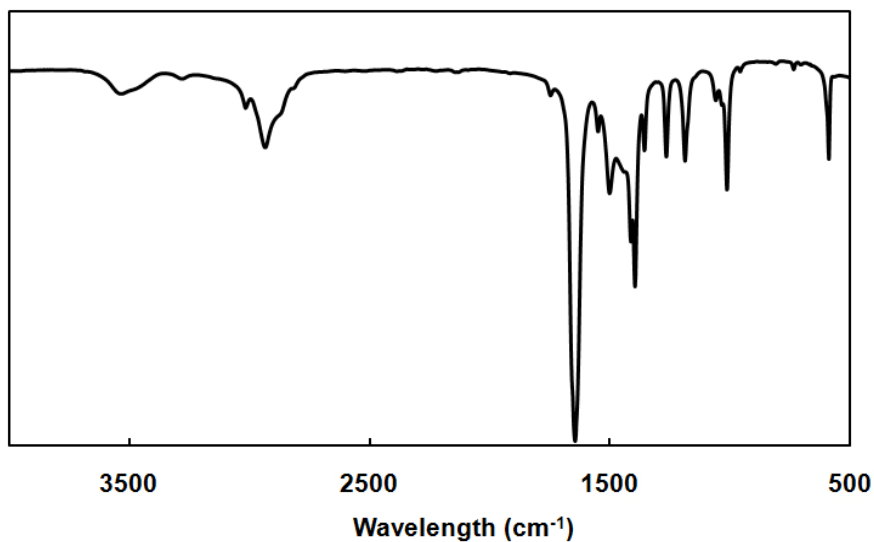


Figure 4. 2 FTIR spectra of PBI

4.1.3. Elemental Analysis

As the structure is seen in Figure 4. 1 the closed formula of PBI is [C₂₀N₄H₁₂]_n. The theoretical percentages of carbon, hydrogen and nitrogen elements in a PBI repeating unit were stated in Table 4.1 as a comparison with data taken experimentally.

The experimental and theoretical values are close to each other. The difference may belong to experimental errors which is ± 3%. Additionally; it is seen that the total percentage of the C, H and N elements of the experimental data is 94.3 %. The residual percentage may be due to the oxygen element in the structure which is caused by

absorbed water throughout the analysis. This absorption justifies the decrease of the C and N percentages and also the increase of the H percentage of the experimental result.

Table. 4.1. The theoretical and experimental values of C, H, N elements in a PBI repeating unit(1 PBI repeating unit:308 g/mol)

%	C	H	N	Impurity (O)
Theoretical	77.92	3.89	18.18	-
Experimental	72.14	4.50	17.66	5.7

4.1.4. Molecular Weight

Molecular weight of the PBI polymer was determined by Ubbelohde viscometer method (Section 3.3.4). For this method; PBI solutions were prepared with concentrations of 1 g/dl; 0.75g/dl; 0.5g/dl and 0.25g/dl in sulphuric acid by diluting. The flow times of the solutions, including the pure solvent, sulphuric acid, were measured through the Ubbelohde viscometer. The measurements were done five times for confirmation.

The specific, reduced, relative and inherent viscosities were calculated by Eqns 3.2 - 3.5. Concentration versus reduced viscosity curve was plotted to obtain the inherent viscosity as shown in Figure 4. 3. (Concentration, inherent viscosity) curve was also plotted for confirmation.

Due to the plot shown in Figure 4. 3 the intrinsic viscosity; $[\eta]$ was determined as 1.89 dl/g. By using the Equation 3.7 molecular weight of the polymer was calculated as 111000.

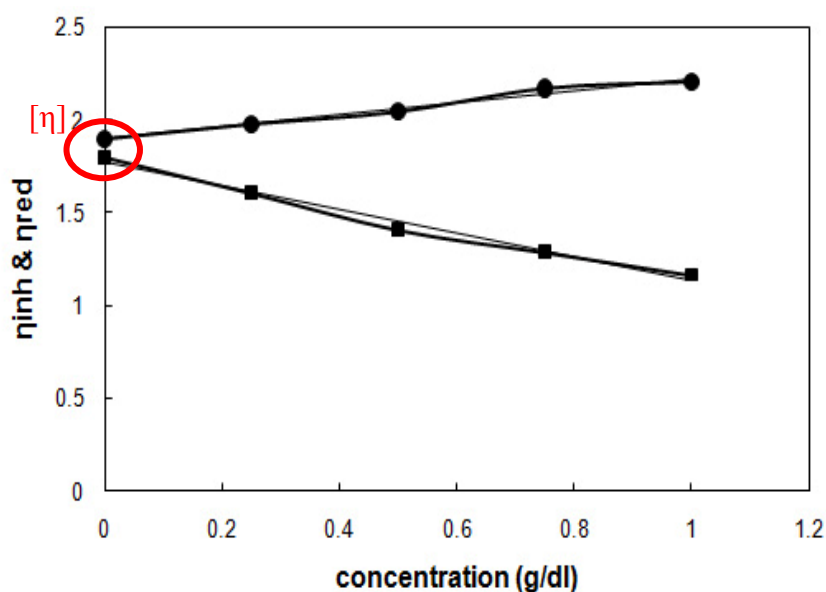


Figure 4. 3 Concentration vs viscosity plot: \bullet : η_{red} ; \blacksquare : η_{inh}

Molecular weights change due to the reaction conditions is shown in Table 4.2. The parameters that affect molecular weight are; reaction time and temperature.

Table 4.2. Reaction conditions, molecular weight and intrinsic viscosities of PBI.

Synthesis No	Reaction temperature (°C)	Reaction time (h)	Intrinsic viscosity (dl/g)	Molecular weight
1	170-200	24	2.0	118500
2	200	24	1.89	111000
3	200	18	1.48	81200
4	185	18	0.46	18700

Molecular weight decreases by decreasing synthesis temperature and also the reaction time. A molecular weight higher than 18000 is necessary for sufficient conductivity and mechanical strength of the membranes (He et al, 2006). Below 18000 the mechanical strength becomes very poor as seen in Figure 4. 4



Figure 4. 4 PBI membrane that is cast from the polymer with a molecular weight of < 18000

Higher molecular weight is required for the PBI in order to increase acid doping level. But at high doping levels the mechanical strength of the

membrane became poor. So the important point is that to work with a polymer with an ideal molecular weight.

By increasing temperature from 185°C to 200°C; molecular weight has increased from 18700 to 81200. At a reaction temperature of 200°C, the molecular weight increased from 81200 to 111000 by increasing reaction time from 18 to 24 hours. A two step solution polymerization (1st step at 170°C, and 2nd step at 200°C) has resulted PBI having the highest molecular weight (118500).

Those results show that the solution polymerization is a successful method to achieve the desired molecular weight of PBI. The second advantage of this method is that the reaction temperature is lower than the melt polymerization which requires 400°C.

Reproducibility

When the polymer synthesis was repeated with the same conditions; the intrinsic viscosity data were obtained approximately same with an ± 0.03 error as it is shown in Table 4.3.

Table 4.3. Reproducibility data of intrinsic viscosities

Synthesis No	Reaction temperature (°C)	Reaction time (h)	Intrinsic viscosity (dl/g)
5	200	24	1.92
6	200	24	1.90
7	200	18	1.45
8	200	18	1.46
9	185	18	0.45
10	185	18	0.48

4.2. Characterization of PBI Membrane

The PBI membranes were prepared with solution casting method by using synthesized PBI polymer and DMAc as solvent. The prepared membranes were doped with phosphoric acid. The acid doped and non-doped membranes were analyzed by FTIR analysis. The thermal and mechanical properties of the membranes were observed by TGA and mechanical analysis respectively.

4.2.1. Fourier Transform Infrared Spectroscopy

The FTIR spectra of PBI membrane and phosphoric acid doped membrane are shown in Figure 4. 5. The spectrum is represented by relatively narrow peaks below 2000 cm^{-1} . These peaks are attributed to

localized normal vibrations of the phenyl groups in the pristine PBI (Musto et al,1993). In the region 2000–1000 cm^{-1} , cycle vibrations as well as the in plane NH and CN deformation modes are expected to occur. According to the spectra shown in Figure 4. 5; in the midwavenumber domain, the region 1500-1650 cm^{-1} is characteristic of benzimidazoles. The benzimidazole characteristic band is clearly observed at 1612 cm^{-1} that is attributed to the C=C/C=N stretching modes (Cordes et al, 1968). Strong absorptions at 1435 and 1531 cm^{-1} result from in-plane deformation of benzimidazole. The breathing mode of the imidazole ring gives a broad band at 1280 cm^{-1} . In-plane C-H deformation vibrations characteristic of substituted benzimidazoles are seen between 1230 and 1090 cm^{-1} . The peaks assigned to the stretching vibrations of the NH and CH groups were detected at 3400 cm^{-1} and 3065 cm^{-1} respectively (Bouchet et al, 1999).

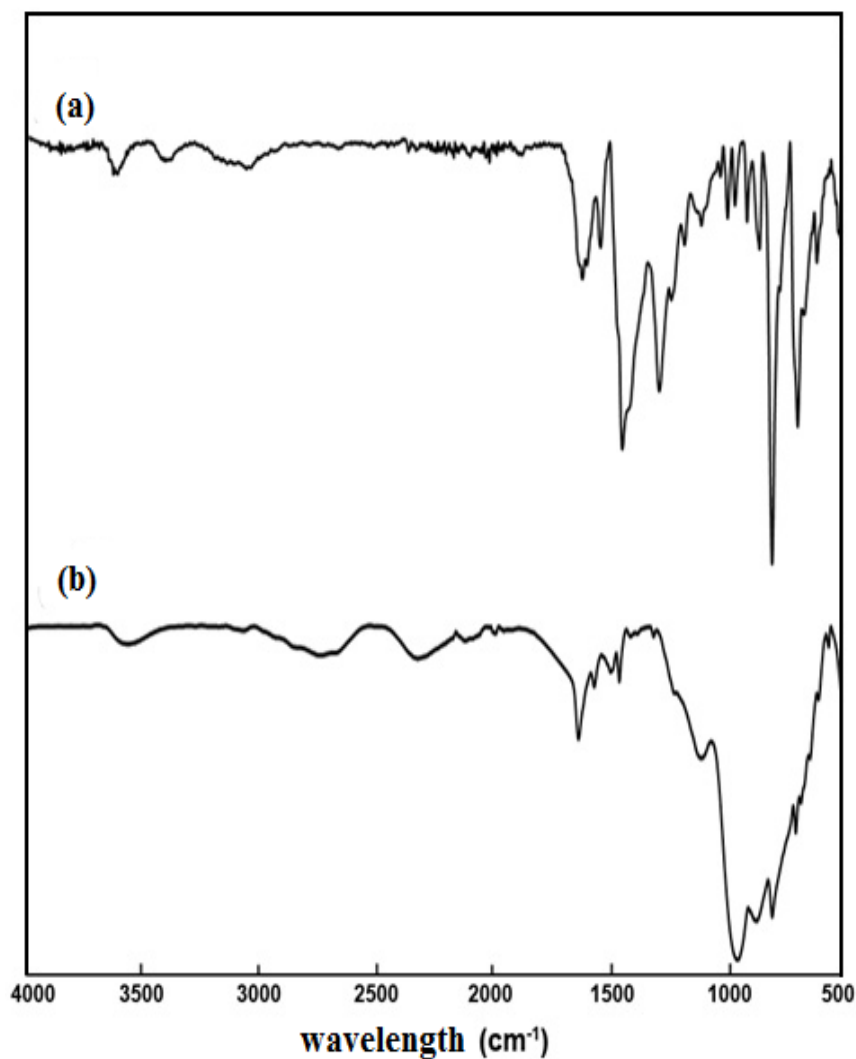


Figure 4. 5. FTIR spectra of a) PBI membrane, b) H₃PO₄ doped PBI membrane.

According to the proton conduction mechanism of H₃PO₄ doped PBI (Section 2.5.2); two regions are expected due to the bonded acid to nitrogens (when doping level is less than 2) and free acids (when doping level is higher than 2). The uptake of phosphoric acid leads to profound spectral modification, in particular in the regions 2000±3500 and 800±1300 cm⁻¹, where wide spectral domains are obscured by absorption

due to hydrogen bonding and vibrations of hydrogen phosphate groups, respectively (Glipta et al, 1999).

A broad band near 2400 cm^{-1} can be attributed to the phosphoric acid that takes place on the imino nitrogen group of the polymer that causes stretching vibration of NH^+ (Wasmus et al, 1995). The addition of phosphoric acid also induces an increase in intensity of bands at 1310, 1457, 1564 and 1632 cm^{-1} , and the appearance of a new signal at 1495 cm^{-1} . This latter band can be attributed to the vibration $\text{C}=\text{N}$ of the $\text{C}=\text{NH}^+$ group, resulting from protonation of the imino nitrogen atom (Glipta, 1999). The broad band complex that appears in the region of about 2500 to 3000 cm^{-1} should be related to the protonation of the nitrogen of the imide by transferring one or two protons from H_3PO_4 to imidazole groups of PBI as shown in the reaction below. This corresponds to the formation of the bonded acid (Li et al, 2004).



4.2.2. X-Ray Diffraction Analysis

PBI has a semi-crystalline structure. The crystallinity is observed by XRD analysis and the XRD patterns of H_3PO_4 doped and undoped PBI membranes are shown in Figure 4. 6.

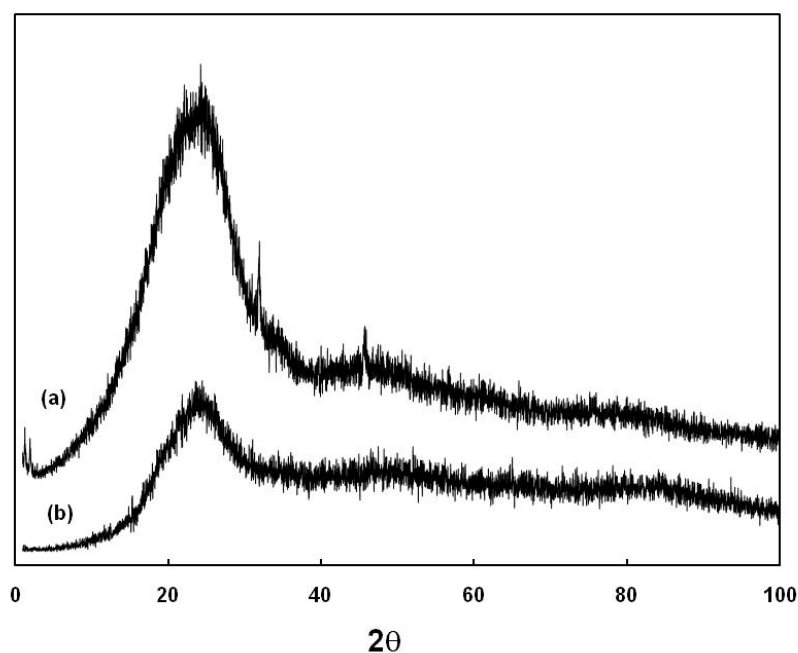


Figure 4. 6. XRD patterns of (a) undoped and (b) H_3PO_4 doped PBI membranes

In the XRD spectra of PBI there is only a single broad peak at about 25° . The peak at 25° corresponds to the spacing between two parallel benzimidazole chains. Wereta et al (1978) observed the parallel stacking of the benzimidazole rings to the film surface (parallel orientation).

When the membranes were doped with the H_3PO_4 , the residual crystalline order is completely destroyed. The films were more amorphous for higher doping content. The observed spectra were in agreement with the results of the literature (Carollo et al, 2006).

4.2.3. Thermal characteristics of PBI membranes

For fuel cell applications, thermal and chemical stability of the membranes are very important. So the thermal stability of the pure PBI membrane and also the H₃PO₄ doped PBI membrane were observed by thermogravimetric (TGA) analysis.

For TGA analysis the samples were heated from 25°C up to 1000 °C with 5 °C/min in a nitrogen atmosphere.

Figure 4. 7 shows the TGA spectra of pristine and H₃PO₄ doped PBI membranes. As shown in Figure 4.7 for pristine PBI membrane (curve (a)); the first weight loss (13 %) can be seen at ~150°C due to the absorbed water. There is no further significant weight loss from 150°C to 500°C which indicates the exceptionally high temperature stability of PBI up to temperatures above 500 °C. The presence of aromatic rings in the PBI structure increases the intermolecular forces, and hence, properties such as thermal stability (Lobato et al, 2006) that can be noticed in the TGA plot.

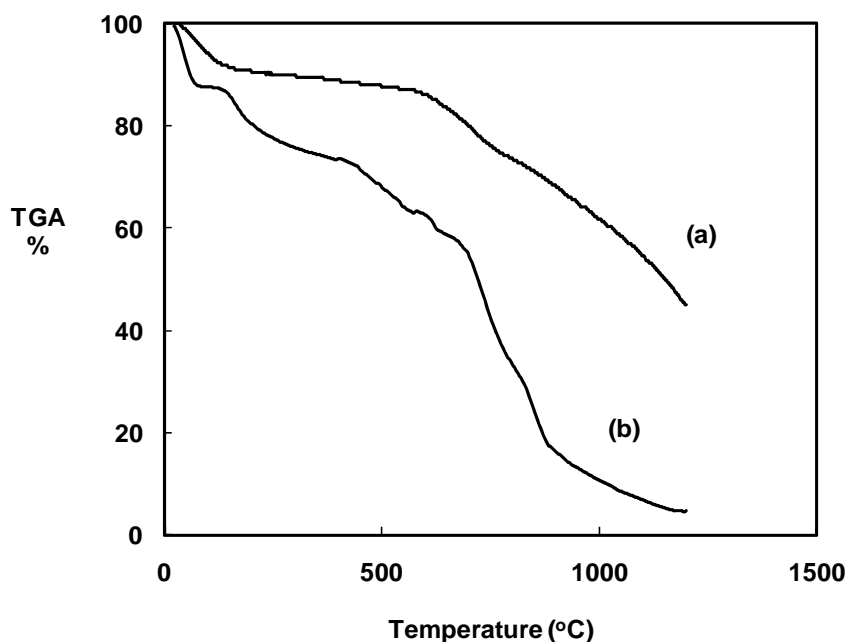


Figure 4. 7 TGA spectra of (a) pristine PBI membrane (b) phosphoric acid doped PBI membrane

The TGA curve of the phosphoric acid doped PBI membrane, that is seen in Figure 4.7 as curve (b), can be explained in three regions. The first weight loss corresponds to the loss of absorbed water at about 110°C. At temperatures above 200°C the second weight loss is observed due to the dehydration of phosphoric acid (Ma et al, 2004) according to the reaction (4.2). After this loss, the next dehydration step of the acid is observed above 600°C due to the reaction (4.3).



Finally the polymer decomposes around 800°C. The weight losses became greater as the membranes doped with acid (Lobato et al, 2006).

4.2.4. The Mechanical Strength of the Membranes

The mechanical strength of the pure PBI membrane is determined by the hydrogen bonding between –N= and –NH– groups. When the membranes are treated with phosphoric acid (doping levels less than 2 molecules of H₃PO₄/repeating unit of PBI) stronger hydrogen bonds between –N= and phosphoric acid molecules are formed (He et al, 2006).

In general the mechanical strength of polymer membranes results from attractive forces between polymer molecules. Among the forces, dipole-dipole interaction is mostly much stronger than London forces and induction interactions. But, when the molecular weight increases, London forces and induction interactions become increasingly significant (Stevens et al, 1999). Consequently the high molecular weighted polymer has better mechanical strength. The membrane cast from the polymer with a molecular weight of 18700 has a stress at break value of 5.5 MPa; since the value is 33 MPa when the molecular weight increased to 111000 as shown in Figure 4. 8 (both membranes were doped with 7 molecules of H₃PO₄/repeating unit of PBI). A negligible decrease was observed when molecular weight decreased from 111000 to 81200.

When polybenzimidazole is doped with phosphoric acid, at doping levels higher than 2, the addition of free acids causes an important deterioration of its mechanical properties (Li et al, 2004). Because when phosphoric acid is introduced in massive amounts in the membrane, free acids get into the matrix and cause a volume swelling, which turns out in a

separation of the PBI polymer chains, with the consequent reduction in the intermolecular forces (He et al, 2006).

The effect of doping level on mechanical strength is seen in Figure 4. 8. As expected when the doping level increases the stress at break decreases. The stress at break value decreased from 33 MPa to 11MPa when doping level increased from 7 to 12. Unfortunately, the weakness of the membrane with a molecular weight of 18700 and doping levels above 7, made extremely difficulty in evaluating their stress at break points. Because the values were below the lower detection limit of the device used.

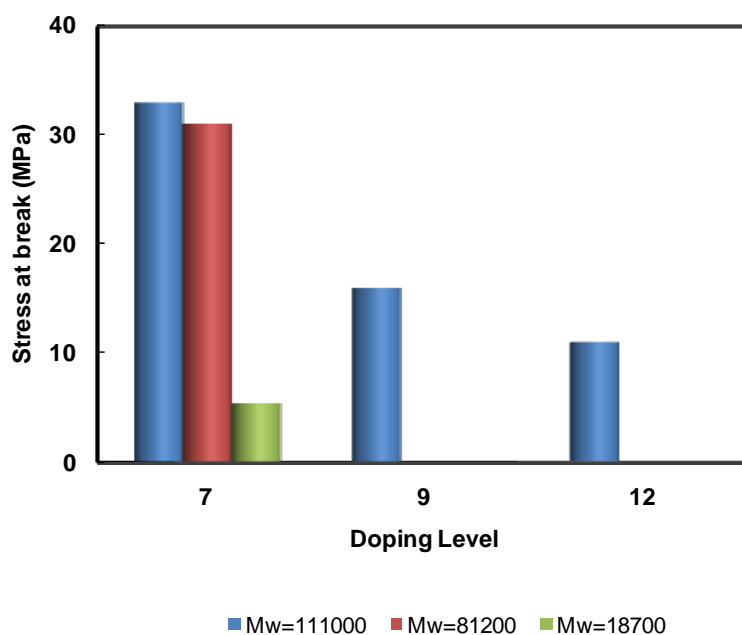


Figure 4. 8 Stress at break values of the PBI membranes for different doping levels and molecular weights. Measurements performed at room temperature and relative humidity.

The reduction of the films mechanical properties when impregnated with the acid and their enhancement with the increase in the molecular weight are clearly observed within this study. The stress strain curves of the membranes that have different doping levels are shown in Figure 4. 9.

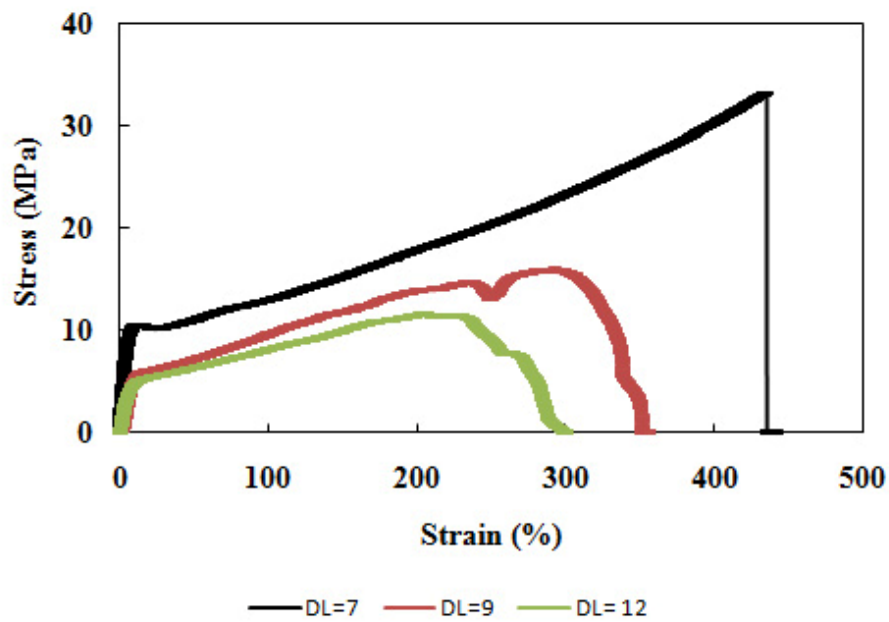


Figure 4. 9 Stress-strain curve of the PBI membranes that have different acid doping levels

4.3. Surface Morphology of the Electrodes

The surface morphology of the electrodes and also the cross sections of the MEAs were studied by Scanning Electron Microscopy (SEM). Energy Dispersive X-ray analysis (EDX) were done on electrode surfaces to observe the Pt distribution homogeneity.

4.3.1. Scanning Electron Microscopy and Energy Dispersive X-ray Analysis of the Electrode Surface

Figure 4. 10 and Figure 4. 11 show top-view SEM scans of the complete electrodes which are prepared by the 1st procedure (Section 3.4.1). The electrodes were doped with phosphoric acid to make an ionic contact between the membrane and electrodes. It is seen in Figure 4. 10.a. and Figure 4. 11.a that the surface is in the mud crack morphology for the electrodes prepared by this procedure. Due to this mud cracked structure, a substantial amount of catalyst is being forced into the crevices when spraying the catalyst layer. The catalyst that entered through the crevices will not contribute to the cell performance (Seland et al, 2006). Additionally as it is seen in Figure 4. 11.b; phosphoric acid deteriorates the surface of the electrode since the surface is covered with the acid film that blocks the pores. The effect of the phosphoric acid on electrode surface can be seen clearly with the comparison of the images Figure 4. 10.b and Figure 4. 11.b which belong to the electrode surfaces that are non-doped and doped, respectively.

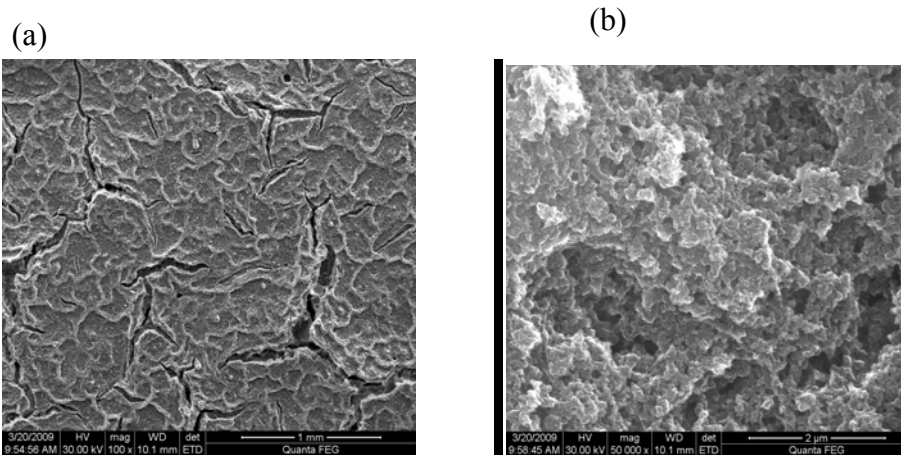


Figure 4. 10 SEM images of non-doped electrode surface (a) with a magnification of (x100) (b) with a magnification of (x50000) (electrodes prepared with 1st procedure)

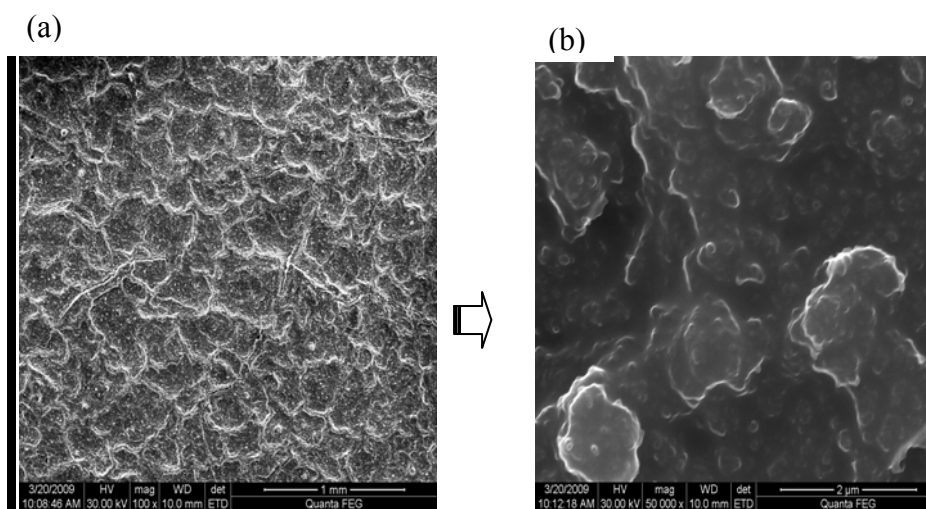


Figure 4. 11 SEM images of H₃PO₄ doped electrode surface (a) with a magnification of (x100) (b) with a magnification of (x50000) (electrodes prepared with 1st procedure)

Figure 4. 12 shows a top-view SEM scan of the complete electrode which is prepared by the 2nd procedure as explained in Section 3.4.1. The surface does not (Figure 4. 12.a) have crevices and the porous structure of the electrode is seen clearly (Figure 4. 12.b). The Pt distributed uniformly on the electrode as it can be seen in Figure 4. 13 from the EDX

(a)

(b)

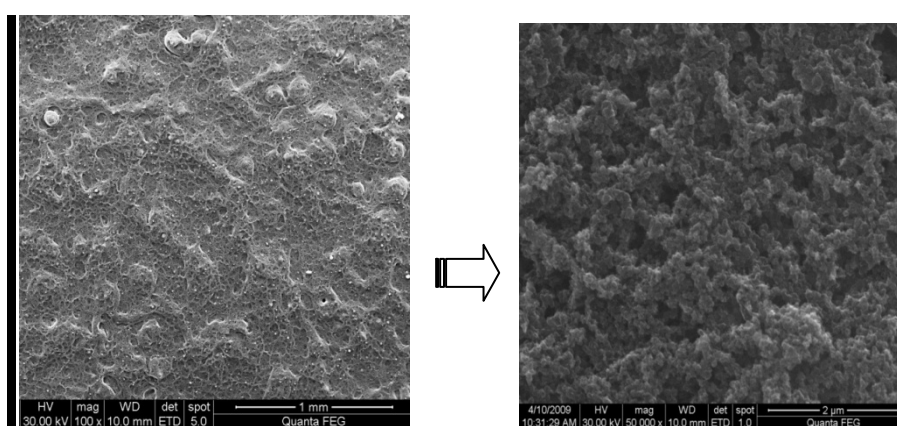


Figure 4. 12 SEM images of non-doped electrode surface in which PBI and PVDF was used as a binder (a) with a magnification of (x100) (b) with a magnification of (x50000) (electrodes prepared with 2nd procedure)

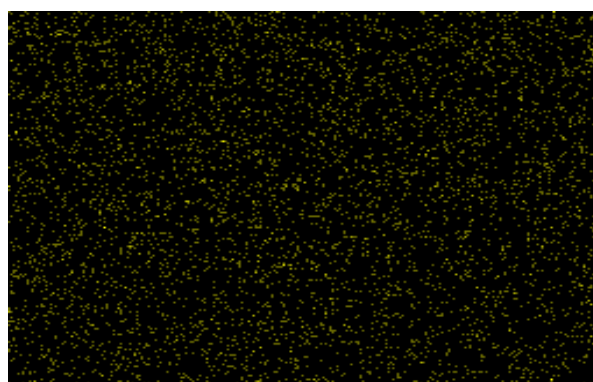


Figure 4. 13 The EDX image of the distribution of Pt on electrode surface

4.3.2. Scanning Electron Microscopy Analysis of the MEA Cross Sections

Several SEM scans of MEA cross-sections were performed in this study. Both secondary electron and backscattered modes were used for scanning. It is preferable to use backscattered mode; because the catalyst layer can easily be seen since platinum shines up due to its high atomic weight. Cross-sections of the MEAs were examined by SEM, before and after testing them in PEM fuel cell. In order to obtain high quality SEM images of the cross-section near the membrane, the MEAs were broken immediately after dipping in liquid nitrogen. SEM scans also show the quality and reproducibility of the spraying technique, which in our case is satisfactorily.

In Figure 4. 14 SEM scans of unused MEAs were seen both in secondary electron and backscattered modes. The catalyst layer can be seen as narrow bright bands on both sides of the membrane. The carbon support layer can also easily be identified as the dark region on the outside of the catalyst layer. SEM images of the cross-section of the respective MEA provides rough estimates of the real thickness of the catalyst layer (Seland et al, 2006) and also membrane thickness. The overall thickness of the catalyst layer and the membrane were measured roughly from the SEM images in Figure 4. 14 to be 20 and 70 μm , respectively. The membrane thickness is measured with a difference of $\pm 5 \mu\text{m}$ through the MEA. This difference is unsatisfactory. It may be due to the hot pressing problems.

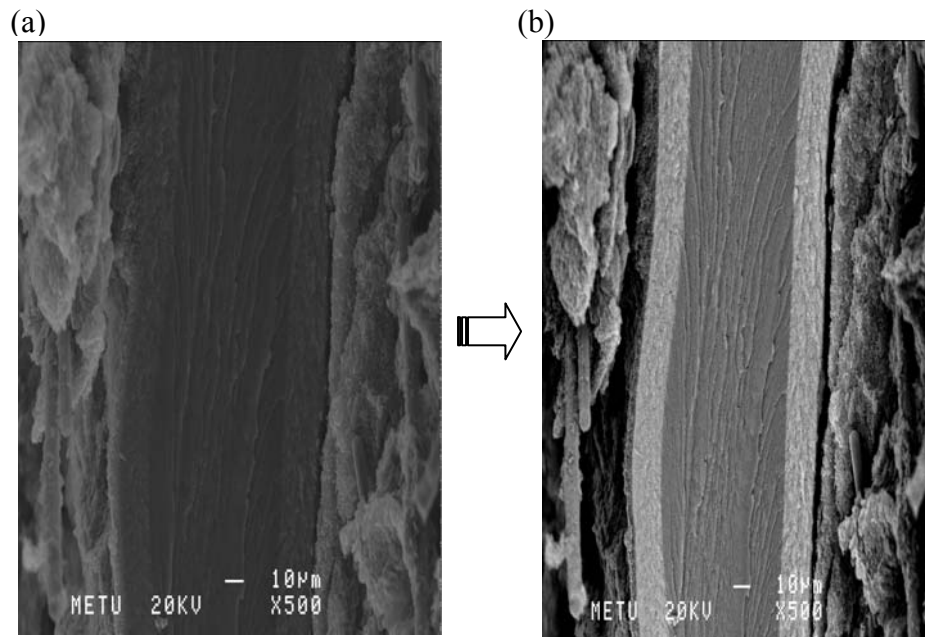


Figure 4. 14 SEM scans of the cross-sections of the unused MEAs prepared by 2nd method (a) in secondary electron and (b) in backscattered mode

In Figure 4. 15 SEM scans of MEAs were seen after testing them in PEM fuel cell. The images are scanned both in secondary electron and backscattered modes. Deformation on catalyst layer is seen briefly as it is marked. More deformations are seen in Figure 4. 16 both on the catalyst layer and also on the membrane cross-section. These deformations shorten the lifetime of the PEMFC.

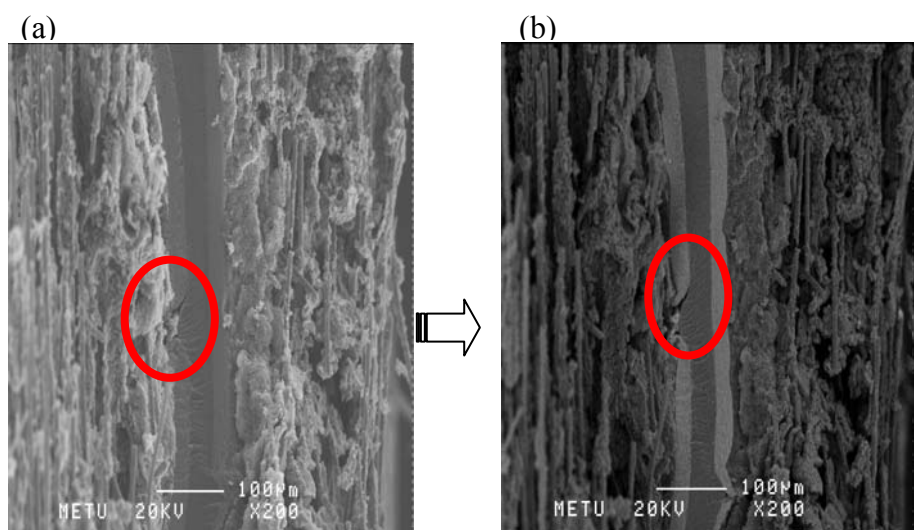


Figure 4. 15 SEM scans of the cross-sections of the MEAs (prepared by 2nd method) after testing in PEMFC (a) in secondary electron (b) in backscattered mode

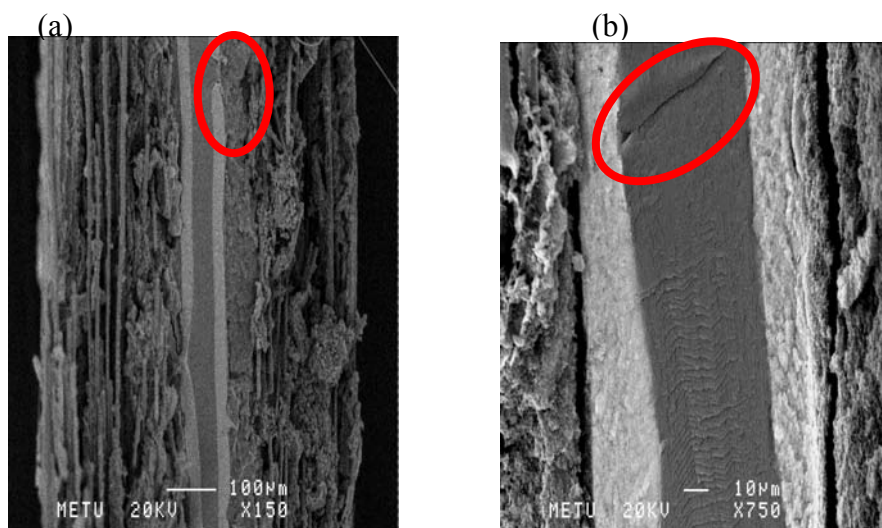


Figure 4. 16 SEM scans of the cross-sections of the MEAs (prepared by 2nd method) after testing in PEMFC in backscattered mode (a) deformation occurred on the catalyst layer (b) deformation occurred on the membrane cross section

4.4. PEMFC Performance Tests

Generally a useful acid doping level can be suggested between 3.5-7.5 mol phosphoric acid for PBI fuel cell performance (Li et al, 2001). In this study PBI membranes with a doping level of 7 (mol H₃PO₄/repeating unit of PBI) were used for performance analysis. To achieve the required phosphoric acid doping level, it is advantageous to cast the membrane from high molecular weighted PBI polymer. Because in high molecular weighted polymer; the number of the bonded phosphoric acid molecules are more and free acids that reduces the mechanical strength are less than in the low molecular weighted ones as explained in Section 4.2.4. According to the Table 4.1 the obtained highest molecular weights are 118500 and 111000, but these polymers had some difficulties in dissolving in DMAc. So the membranes which are cast from polymers with molecular weights of 81200 were used for performance analysis.

The prepared MEAs were placed in the PEM fuel cell which has an active area of 5 cm². The temperatures of the cell and also the gas transfer lines were set to the required values. Before feeding of reaction gases, nitrogen was sent to the anode part of the cell for 10-15 minutes to understand if there is a leakage through the membrane. After nitrogen test, dry hydrogen and oxygen gases were fed to the anode and cathode sides of the cell respectively; at a flow rate of 0.1 slpm.

The effects of the binder used in the catalyst ink, membrane thickness and operating temperature were studied throughout this study. They are explained in this part in details and the scope of the experiment conditions and the obtained data are summarized in Section 4.5 within the Table 4.3.

4.4.1. Effect of binder used in the catalyst ink on PEMFC Performance

The performance curves of the MEAs which were prepared by the 1st procedure are shown in Figure 4. 17. The effect of phosphoric acid concentration that doped to the electrodes were observed. As it is seen; when the phosphoric acid concentration was decreased from 85wt.% to 50wt.% the max power output of the cell is increased considerably from 0.0042 W/cm² to 0.0145 W/cm². So it seems to use a low concentrated H₃PO₄ is more advantageous. But at that time when 25wt.% H₃PO₄ was used, hot pressing problems occurred. The electrode cannot stick to the PBI membrane surface and consequently any performance could not be achieved by the not-pressed MEA. So it is concluded that the preferable concentration of H₃PO₄ for electrode doping is 50wt %.

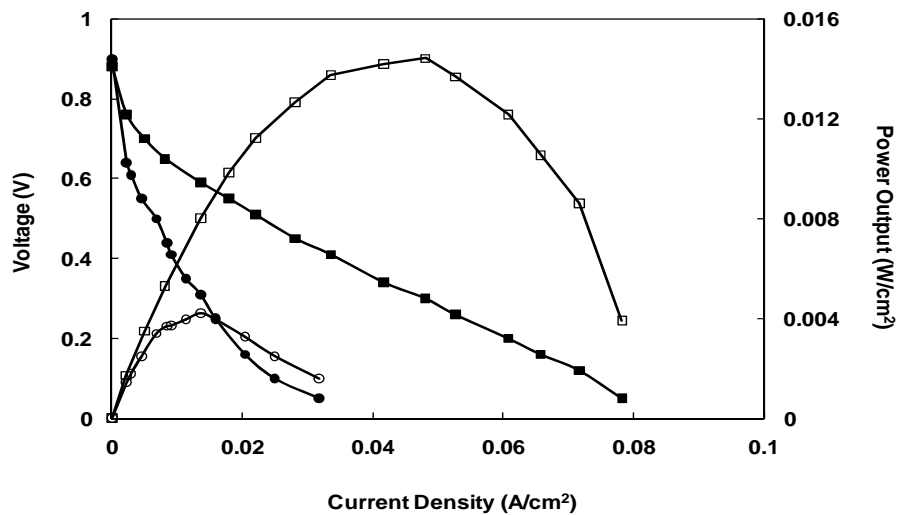


Figure 4. 17 PBI performance curves at 150°C (polarization-closed symbols; power-open symbols) —●—, —○—: electrodes doped by 85 % H₃PO₄; —■—, —□—: electrodes doped by 50 % H₃PO₄.

As it was mentioned in the experimental part; PVDF and PBI solutions were used as the binder in the catalyst ink as 2nd procedure of MEA preparation. In performance analysis the effect of the PVDF amount in the catalyst ink was observed. In this sense; the ratio of PVDF to PBI was changed and its effect on performance was observed. As it is seen in Figure 4. 18 the maximum output was increased from 0.057 W/cm² to 0.061 W/cm², 0.072 W/cm² as the PVDF:PBI ratio goes from 1:3 to 3:1 respectively. So it is clear that PVDF in the catalyst ink has an increasing effect on performance. But as the time passes it was observed that the performance was dropped in a short time (about 20 hours) when PVDF amount is high in the catalyst ink. Moreover; the OCV value is decreased from 1 V to 0.84 V when the PVDF:PBI ratio is changed as 3:1. The decrease of the OCV and low current performance are caused by hydrogen crossover that causes the mixing of the reactant species before they have had a chance to participate in the electrochemical reaction (Barbir, 2003). So it is concluded that it is preferable to keep on the performance studies with the electrodes that have a PVDF:PBI ratio as 1:3 in the catalyst ink.

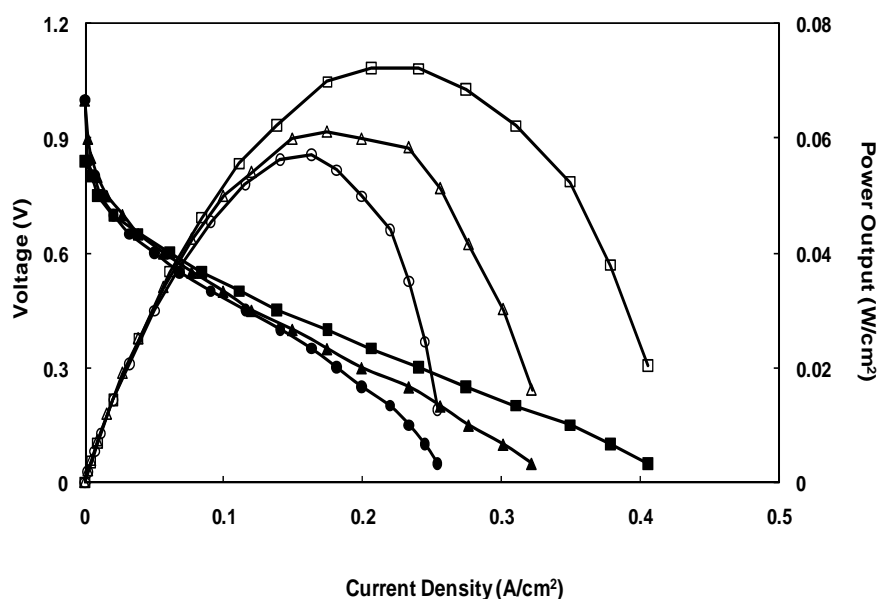


Figure 4. 18 PBI performance curves (polarization-closed symbols; power-open symbols) of the electrodes with a binder of: \bullet , \circ : PVDF:PBI=1:3; \blacktriangle , \triangle : PVDF:PBI=1:1; \blacksquare , \square : PVDF:PBI=3:1 (at 150°C)

4.4.2. Effect of Temperature on PEMFC Performance

The effect of temperature is very important for fuel cell performances. In general a higher cell temperature results in a higher cell potential (Figure 4.19). This is because of the voltage losses in operating fuel cells decrease with temperature. Open circuit potential of the membrane was 1 V which was quite acceptable for PEM fuel cells as stated in the literature as 0.90 V (Lobato et al, 2006), 0.87 V (Zhang et al, 2007) and 0.85 V (Kongstein et al, 2007). The fuel cell has reached to the maximum power of 0.063 W/cm² at 160°C. Lobato et al (2006) obtained a maximum power output of 0.085 W/cm² at 125°C and 0.14 W/cm² at 150°C. Additionally Li et al (2001) achieved a maximum power output of

0.36 W/cm² at 170°C. It can be seen that the performance gets better at higher temperatures due to the higher electrolyte conductivity and the faster electrochemical reaction processes. Kongstein et al (2007) observed a nearly linear increase of power density with increasing temperature, indicating the benefit of high-temperature operation. For higher performance of the PBI membranes; operation at higher temperatures and also higher doping levels of membranes will be a focus of our on-going studies.

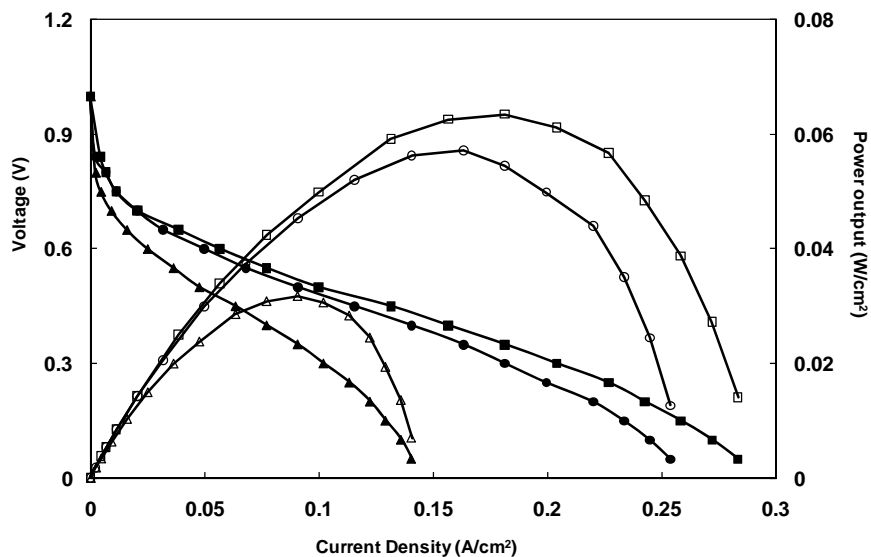


Figure 4.19 PBI performance curves (polarization-closed symbols; power-open symbols) for different temperatures: —▲, —△: 125°C; —●, —○: 150°C; —■, —□: 160°C

4.4.3. Effect of Membrane Thickness on PEMFC Performance

Thickness of the membrane has also a serious effect on performance. As it is seen in Figure 4.20, the single-cell test presents a current density of about 56 mA/cm² and 43 mA/cm² at a cell voltage of 0.6 V with

membrane thicknesses of 70 and 100 μm , respectively. The obtained higher performances with thinner membranes is an expected result as the proton transfer from anode to cathode gets easier as the membrane becomes thinner.

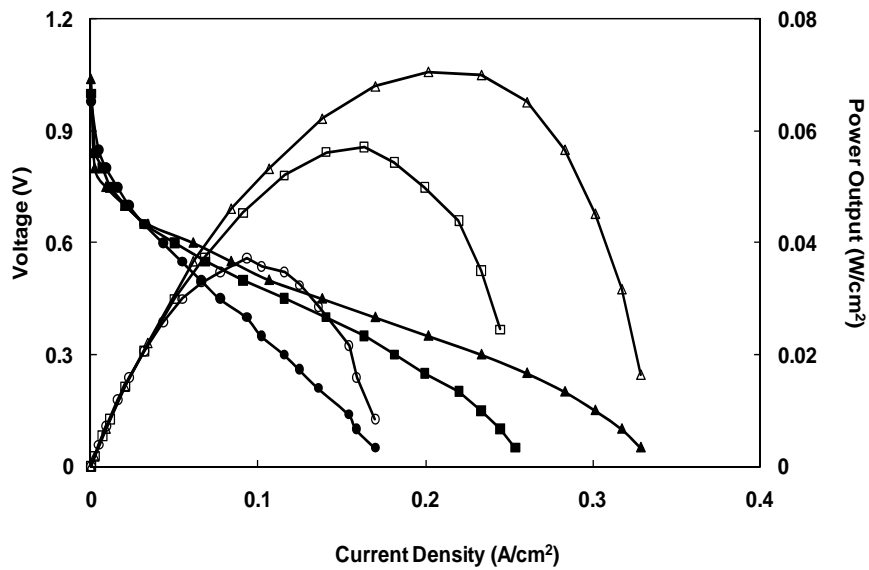


Figure 4.20 PBI performance curves (polarization-closed symbols; power-open symbols) of the membranes with a thickness of: \bullet , \circ : 100 μm ; \blacksquare , \square : 80 μm ; \blacktriangle , \triangle : 70 μm (at 150°C)

4.4.4. The Effect of Operating Time on Fuel Cell Performance

Generally fuel cells operate between 0.4-0.6 volts. So the power output data at these voltages were taken by time in Figure 4.21. An increase is seen up to around 20 hours due to activation and also for the time necessary for bridging the proton conduction mechanism. After 44 hours a decrease in cell potential was observed due to the phosphoric acid loss of the membrane in addition to the time required for stabilization.

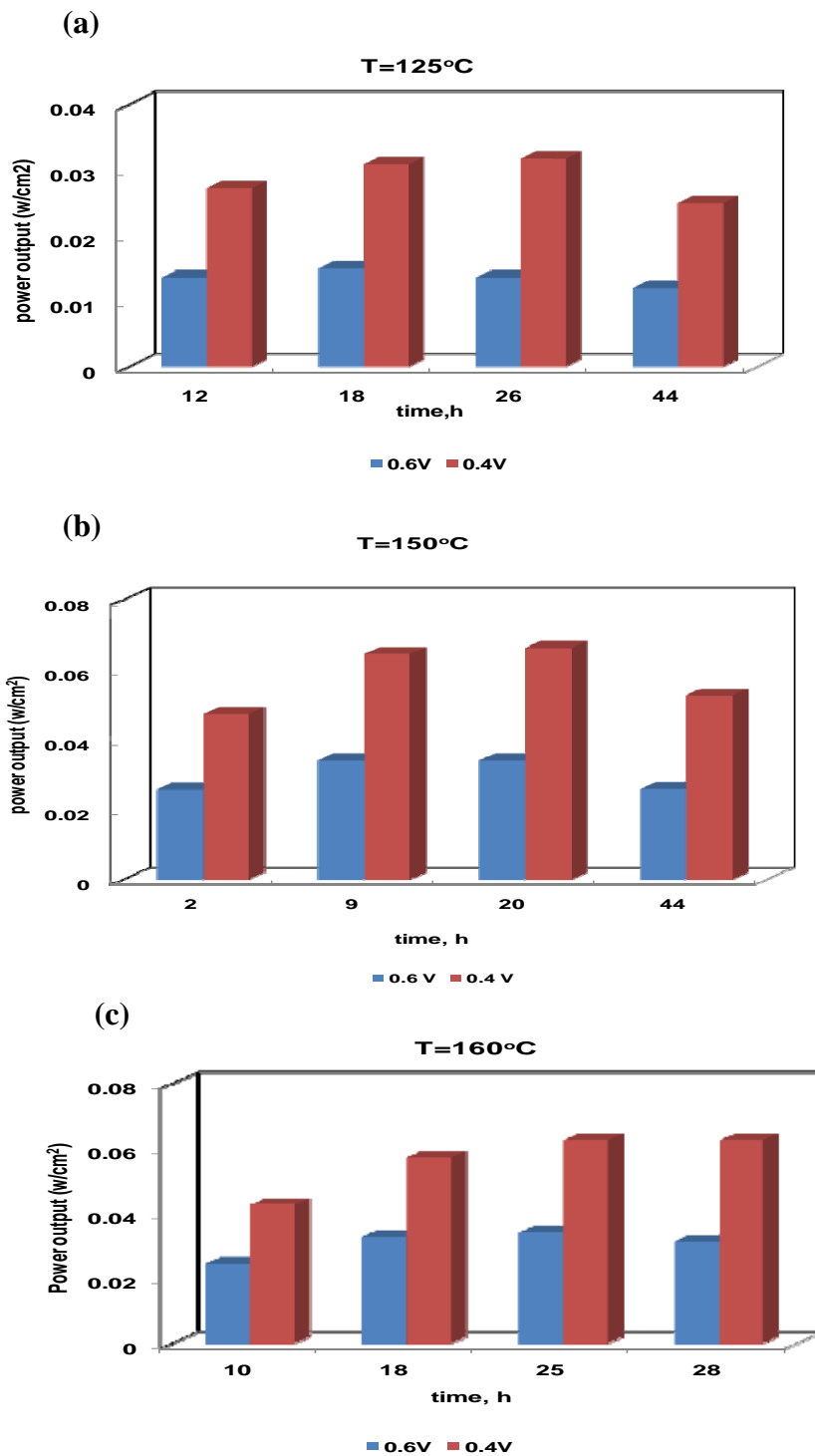


Figure 4. 21 Time dependence of fuel cell performance (a) 125°C (b) 150°C (c) 160°C

Li (2005) was reported a stable performance of a PBI/H₂O₂ fuel cell at 150°C for 5000 hours. A thermal cycling test with a daily shut down and restart was performed by their group.

It can be concluded that a test station must be developed for lifetime tests and some procedures should be applied to extend the lifetime. Afterwards the eventual loss of the doping acid and oxidative degradation of the polymer should be the major concern with respect to the lifetime of the acid doped PBI membranes under fuel cell operation (Li, 2005).

4.5. Summary of the PEM Fuel Cell Performance Analysis

It is concluded that it is preferable to use both PVDF and PBI solutions, in the ratio of PVDF:PBI= 1:3, as the binder in catalyst ink to be sprayed onto the electrodes. The performance increases as temperature increases and membrane thickness decreases. The conditions and the obtained data are summarized in Table 4.4.

Table 4. 4 Test Conditions and output data of performed experiments for fuel cell performance tests (*The darkened lines are the preferable conditions.)

Test Condition	PVDF:PBI ratio in catalyst ink	Temperature (°C)	Thickness (µm)	OCV (V)	Max. Power Output (W/cm ²)
1	0:1 (electrodes doped with 85% H ₃ PO ₄)	150	80	0.9	0.0042
2	0:1 (electrodes doped with 50% H ₃ PO ₄)	150	80	0.88	0.0145
*3	1:3	150	80	1	0.057
4	1:1	150	80	1	0.061
5	3:1	150	80	0.84	0.072
6	1:3	125	80	1	0.032
7	1:3	160	80	1	0.063
*8	1:3	150	70	1.04	0.070
9	1:3	150	100	0.98	0.035

CHAPTER 5

CONCLUSIONS AND RECOMMENDATIONS

The objective of the study was to develop phosphoric acid doped polybenzimidazole membranes for high temperature (100-150°C) operation of PEM fuel cells. Therefore in the present work, PBI polymers with different molecular weights were synthesized. The synthesis conditions were changed to obtain different molecular weighted polymer. Polymerization time and temperature were taken as synthesis parameters. When the polymerization was done at 185°C for 18 hours PBI was obtained with a molecular weight of 18700. Molecular weight was increased to 111000 (about 5 times of the previously mentioned one) when the time and temperature was increased to 24 hours and 200°C, respectively. So it is concluded that molecular weight of the polymer increases as reaction time and temperature increases. For fuel cell applications it is advantageous to use high molecular weighted polymer since its better mechanical properties. But as the molecular weight increased up to 120000, the solubility of the polymer in DMAc becomes so difficult. So the preferable molecular weight range was determined as 81200-111000 with sufficient mechanical stability and also availability of easy dissolving in DMAc.

The polymer was characterized by Fourier Transform Infrared Spectroscopy (FTIR) and Proton- Nuclear Magnetic Resonance (H-

NMR) spectroscopy. Characteristic peaks of benzimidazole chains were observed briefly which are in agreement with the literature. As the result of elemental analysis, it is found that the theoretical and experimental percentages of the C, H and N elements in the PBI chain were so close to each other. So the characterization analysis were satisfactory that concludes the successful synthesis of PBI.

The synthesized PBI polymers were suitable to prepare homogeneous membranes that have high mechanical and thermal stability. The PBI membranes must be doped with phosphoric acid to have sufficient proton conductivity thus fuel cell performance.

The thermal and mechanical stabilities of PBI and acid doped PBI membrane have been studied by thermogravimetric and mechanical analysis respectively. The TGA analysis indicates the exceptionally high temperature stability of PBI up to temperatures above 500°C. The membrane cast from the polymer with a molecular weight of 18700 has a stress at break value of 5.5 MPa; since the value is 33 MPa when the molecular weight increased to 110000 (both membranes were doped with 7 molecules of H₃PO₄/repeating unit of PBI). A negligible decrease was observed when molecular weight decreased from 111000 to 81200. The stress at break value decreased from 33 MPa to 11 MPa when doping level increased from 7 to 12. So it is concluded that mechanical strength increases with increasing molecular weight and decreasing acid doping level. So the fuel cell performance tests were done with the membranes that are doped with 7 molecules of H₃PO₄/repeating unit of PBI as the preferable value.

Acid doped PBI membrane and the pristine membrane was also characterized by X-Ray Diffraction (XRD) analysis. Just looking at the peaks obtained, the destruction of the crystalline order is seen briefly when the membranes were doped with phosphoric acid.

The technique developed during the present work, to spray the catalyst ink onto GDL, is an appropriate method for the preparation of the electrodes. It should be emphasized that the best binder for assembling the electrodes and the PBI membrane was PBI (5 wt %) and PVDF (1 wt %) in DMAc solutions that was mixed to the catalyst ink. The catalyst ink should be sprayed onto the GDL until the desired Pt loading is achieved (0.4 mg Pt/cm^2).

The surface morphology of the PBI based electrodes and also the cross sections of the MEAs were examined by SEM analysis. It was seen that the surface of the electrode was in the mud crack morphology for the electrodes prepared with the binder of PBI (1st procedure). Due to this mud cracked structure, a substantial amount of catalyst was being forced into the crevices when spraying the catalyst ink. The catalyst that entered through the crevices could not contribute to the cell performance. But when PVDF was used as the binder in addition to PBI in catalyst ink, an improvement was observed in the surfaces. The homogeneous Pt distribution on electrode surfaces were observed by EDX analysis which is also satisfactory for the present study. For the SEM images of the cross sections of MEAs, backscattered mode was preferable as the Pt shines due to its high atomic value. It is clearly seen that some deformations occurred on the catalyst layer and also on the membrane surface after testing them in the PEMFC. It must be

emphasized that these deformations must be improved for durability studies.

The PBI membrane-electrode assemblies that were tested in the fuel cell test station did not require any humidification of oxygen and hydrogen gases. The performance of the PBI membranes were tested in a single cell and parameters such as binder, membrane thickness etc, that affects the performance were observed.

During the study; it was achieved to operate the single cell up to 160°C. The observed maximum power output was increased considerably from 0.015 to 0.061 W/cm² at 150°C when the binder of the catalyst was changed from polybenzimidazole to polybenzimidazole and polyvinylidene fluoride mixture. The power outputs of 0.032 and 0.063 W/cm² were obtained when the fuel cell operating temperatures changed as 125 and 160°C respectively. The single cell test presents a maximum power out of about 0.035 and 0.070 W/cm² with membrane thicknesses of 100 and 70 μm respectively. So it can be concluded that thinner membranes give better performances at higher temperatures.

A decrease was observed in fuel cell potential after operating 44 hours. The reason was attributed to the loss of phosphoric acid in PBI membrane.

Recommendations:

- The reasons for performance loss by time can be investigated.

- A test station can be set up just for the life time tests of PBI membranes.
- Modelling of a PEMFC with PBI membrane can be developed.

REFERENCES

Akay, R. G. *Development and characterization of composite proton exchange membranes for fuel cell application*, PhD Thesis, METU, Ankara, 2008.

Barbir, F., *Handbook of Fuel Cell Technology-Fundamentals, Technology and Applications* (Vol. 4), (W. Vielstich, A. Lamm, & H. Gasteiger, Eds.) New York: J.Wiley, 2003.

Barbir, F., *PEM Fuel Cells: Theory and Practice*, Elsevier Academic Press, 2005.

Bayrakçeken, A., *Platinum and Platinum-Ruthenium Based Catalysts on Various carbon Supports Prepared by Different Methods for PEM Fuel Cell Applications*, PhD Thesis, METU, Ankara, 2008.

Bayrakçeken, A., Erkan, S., Türker, L., & Eroğlu, İ., Effects of membrane electrode assembly components on proton exchange membrane fuel cell performance, *Int J Hydrogen Energy* (2008), pp. 165–170.

Bouchet, R., & Siebert, E., Proton Conduction in Acid Doped Polybenzimidazole, *Solid State Ionics* 118 (1999), pp. 287-99.

Buckley, A., Stuetz, D., & Serad, G., Polybenzimidazoles, *Encyclopedia of Polymer Science and Engineering*, Wiley, 1987 .

Carollo, A., Quartarone, E., & Tomasi, C., Developments of new proton conducting membranes based on different polybenzimidazole structures for fuel cells applications, *Journal of Power Sources* 160 (2006), pp. 175-80.

Chuang, S.-W., Hsu, S., Synthesis and Properties of a New Fluorine-Containing Polybenzimidazole for High-Temperature Fuel-Cell Applications, *Journal of Polymer Science: Part A: Polymer Chemistry*, 44 (2006), pp. 4508-13.

Davies, D., Adcock, P., Turbin, M., & Rowen, S., Stainless Steel as a Bipolar Plate Material for Solid Polymer Fuel Cells, *Journal of Power Sources* 86 (2000), pp. 237-42.

Devrim, Y., Erkan, S., Baç, N., & Eroğlu, İ., Preparation and characterization of süsfonated polysulfone/titanium dioxide composite membranes for proton exchange membrane fuel cells, *International Journal of Hydrogen Energy* 34 (2009), pp. 3467-75.

Erdener, H., *Development of organic-inorganic composite membranes for fuel cell applications*, Ms Thesis, METU, Ankara, 2007.

Erkan, S., *Synthesis of Some Metalophthalocyanines and Their Effects on the Performance of PEM Fuel Cells*, Ms Thesis, METU, Ankara, 2005.

Gang, X., Qingfeng, L., Hjuler, H., & Bjerrum, N., Hydrogen Oxidation on Gas Diffusion Electrodes for Phosphoric Acid Fuel Cells in the Presence of Carbon Monoxide and Oxygen, *Journal of Electrochem. Soc.* 142 (1995), pp. 2890.

Glipa, X., Bonnet, B., Mula, B., Jones, D., & Rozieare, J., Investigation of the conduction properties of phosphoric and sulfuric acid doped polybenzimidazole, *J. Mater. Chem.* 9 (1999), pp. 3045-49.

Grove, W., On voltaic series and the combination of gases with platinum, *Philosophical Magazine* 14 (1839), pp. 127.

He, R., Li, Q., Bach, A., & Jensen, J., Physicochemical properties of phosphoric acid doped polybenzimidazole membranes for fuel cells, *Journal of Membrane Science* 277 (2006), pp. 38-45.

Iwakura, Y., Uno, K., & Imai, Y., Polyphenylenebenzimidazoles, *Journal of Polymer Science: PART A*, 2 (1964), pp. 2605-2615.

Kadirov, M., Bosnjakovic, A., & Schlick, S., Membrane-derived fluorinated radicals detected by electron spin resonance in UV irradiated Nafion and Dow ionomers: effect of counterions and H₂O₂, *Journal of Physical Chemistry B* 109 (2005), pp. 7664-7666.

Kakaç, S., Pramuanjaroenkij, A., & Vasiliev, L., *Mini Micro Fuel Cells Fundamentals and Applications*, Springer, 2007.

Kojima, T., Proton NMR Studies of a Polybenzimidazole in Solution, *Journal of Polymer Science: Polymer Physics Edition*, 18 (1980), pp. 1791-1800.

Kongstein, O., Berning, T., Borresen, B., Seland, F., & Tunold, R., Polymer electrolyte fuel cells based on phosphoric acid doped polybenzimidazole (PBI) membranes, *Energy* 32 (2007), pp. 418-22.

Kuang, K., & Easler, K., *Fuel Cell Electronics Packaging*. San diego: Springer, 2007.

LaConti, A., & Hamdan, M. M., *Handbook of fuel Cells: Fundamentals, Technology, and Applications* (Vol. 3). England: John Wiley and Sons, 2003.

Li, M., Shao, Z., & Scott, K., A high conductivity Cs_{2.5}H_{0.5}PMo₁₂O₄₀/ polybenzimidazole (PBI)/H₃PO₄ composite membrane for proton-exchange membrane fuel cells operating at high temperature, *Journal of Power Sources* (2008), pp. 69-75.

Li, Q., *High Temperature Proton Exchange Membranes for Fuel Cells*, PhD Thesis, Technical University of Denmark, 2005.

Li, Q., He, R., Berg, R., Hjuler, H., & Bjerrum, N., Water uptake and acid doping of polybenzimidazoles as electrolyte membranes for fuel cells, *Solid state Ionics* 168 (2004), pp. 177-85.

Li, Q., He, R., Jensen, J., & Bjerrum, N., PBI-Based Polymer Membranes for High Temperature Fuel Cells- Preparation, Characterization and Fuel Cell Demonstrations, *Fuel Cells* 4 (2004), pp. 147-59.

Li, Q., Hjuler, H., & Bjerrum, N., Phosphoric acid doped polybenzimidazole membranes: Physiochemical characterization and fuel cell applications, *Journal of Applied Electrochemistry* 31 (2001), pp. 773-9.

Li, X., *Principles of Fuel Cells*, New York: Taylor & Francis Group, 2006.

Lobato, J., Rodrigo, M., & Manjavacas, G., Synthesis and characterisation of poly[2,2-(m-phenylene)-5,5-bibenzimidazole] as polymer electrolyte membrane for high temperature PEMFCs, *Journal of Membrane Science* 280 (2006), pp. 351-62.

Ma, Y., *The fundamental studies of polybenzimidazole/phosphoric acid electrolyte for fuel cells*, PhD thesis in Chemical Engineering, Case Western Reserve University, Ohio, USA, 2004.

Ma, Y., Wainright, J., Litt, M., & Savinell, R., Conductivity of PBI membranes for high-temperature polymer electrolyte fuel cells, *Journal of Electrochem. Soc.* 151, (2004), pp. A8-A16.

Mench, M., *Fuel Cell Engines*. Wiley, 2008.

Olabisi, O., & Marcel, D., *Handbook of Thermoplastics*, New York, 1996.

Panchenko, A., Polymer Electrolyte Membrane Degradation and Oxidant Reduction in Fuel Cells: an EPR and DFT investigation, *PhD Thesis*, Institute für Phyzikalische Chemie der Universitat, 2004.

Quian, R., The molecular weight measurement of polymer, *Beijing:Science Press* (1958), pp. 41.

Sannigrahi, A., Arunbabu, D., Sankar, R., & Jan, T., Aggregation Behavior of Polybenzimidazole in Aprotic Polar Solvent, *Macromolecules*, 40 (2007), pp. 2844-51.

Schönberger, F., Hein, M., & Kerres, J., Preparation and characterisation of sulfonated partially fluorinated statistical poly(arylene ether sulfone)s and their blends with PBI, *Solid State Ionics* 178 (2007), pp. 547-54.

Schuster, M., Meyer, W., Schuster, M., & Kreuer, K., Toward a new type of anhydrous organic proton conductor based on immobilized imidazole, *Chem. Mater.* 16 (2004), pp. 329–37.

Seland, F., Berning, T., Borresen, B., & Tunold, R., Improving the Performance of High Temperature PEM Fuel Cells Based on PBI Electrolyte, *Journal of Power Sources* 160 (2006), pp. 27-36.

Shogbon, C., Brousseau, J., Zhang, H., Benicewicz, B., & Akpalu, Y., Determination of the molecular parameters and studies of the chain conformation of polybenzimidazole in DMAc/LiCl, *Macromolecules* 39 (2006), pp. 9409-18.

Stevens, M., *Polymer chemistry: An introduction* (3rd Edition:62 ed.), New York: Oxford University Press, 1999.

Sukumar, P., *New Proton Conducting Membranes for Fuel Cell Applications*, PhD thesis, India, 2006.

Şengül, E., *Preparation and Performance of Membrane electrode Assemblies with Nafion and Alternative Polymer Electrolyte Membranes*. Ms Thesis, METU, Ankara, 2007.

Vogel, H., & Marvel, C., Polybenzimidazoles, new thermally stable polymers, *Journal of Polymer Science*, (1961) pp. L:511-39.

Wainright, J., Wang, J., Weng, D., Savinell, R., & Litt, M., Acid-doped polybenzimidazoles: A new polymer electrolyte, *J. Electrochem. Soc.* 142 (1995), pp. 121-3.

Weast, R., *CRC Handbook of Chemistry and Physics*. Boca Raton: CRC Press, 1988.

Weng, D., *Water and methanol transport through polymer electrolytes in elevated temperature fuel cells*, PhD Thesis, Case Western Reserve University, Cleveland, 1996.

Wereta, A., & Gehatia, M. T., Morphological and physical property effects for solvent cast films of poly-2,5(6) benzimidazole, *Polym. Eng. Sci.* 18 (1978), pp. 204-9.

Williams, M., Begg, E., Bonville, L., Kunz, H., & Fenton, J., Characterization of Gas Diffusion Layers for PEMFC, *Journal of Electrochem Soc* 151, (2004), pp. A1173-80.

Xiao, L., Zhang, H., Scanlon, E., Ramanathan, L., Choe, E., Rogers, D., High temperature polybenzimidazole fuel cell membranes via a sol-gel process, *Chem. Mater.* 17, (2005), pp. 5328-33.

Xing, B., & Savadogo, O., The effect of acid doping on the conductivity of polybenzimidazole (PBI), *Journal of New Materials for Electrochemical systems* 2 (1999), pp. 95-101.

Yurdakul, A. Ö., *Acid-doped polybenzimidazole membranes for high temperature proton exchange membrane fuel cells*, MS Thesis, METU, Ankara, 2007.

Zaidi, J., & Matsuura, T., *Polymer Membranes for Fuel Cells*, Springer, 2009.

Zenith, F., *Control of fuel cells*, PhD thesis, Trondheim, 2007.

Zhang, J., *PEM Fuel Cell Electrocatalysts and Catalyst Layers, Fundamentals and Applications*, Canada: Springer, 2008.

Zhang, J., Tang, Y., & Song, C., Polybenzimidazole-membrane-based PEM fuel cell in the temperature range of 120–200 °C, *Journal of Power Sources* 172 (2007), pp. 163-71.

Zhang, J., Zhong, X., Tang, Y., & Song, C., High Temperature PEM Fuel Cells. *Journal of Power Sources* 160 (2006), pp. 872-91.

APPENDIX A

Phosphoric acid doping to PBI membranes

Sample Calculation of acid doping level :

According to the Eq. 3.1;

$$\begin{aligned} \text{Acid doping} &= \frac{(0.35 - 0.073) \text{g H}_3\text{PO}_4}{0.073 \text{ g PBI}} \times \frac{308 \text{ gPBI/RU of PBI}}{98 \text{ g H}_3\text{PO}_4/\text{mol H}_3\text{PO}_4} \\ &= 12 \text{ mol H}_3\text{PO}_4 / \text{Repeating unit of PBI} \end{aligned}$$

Doping Level changing by time:

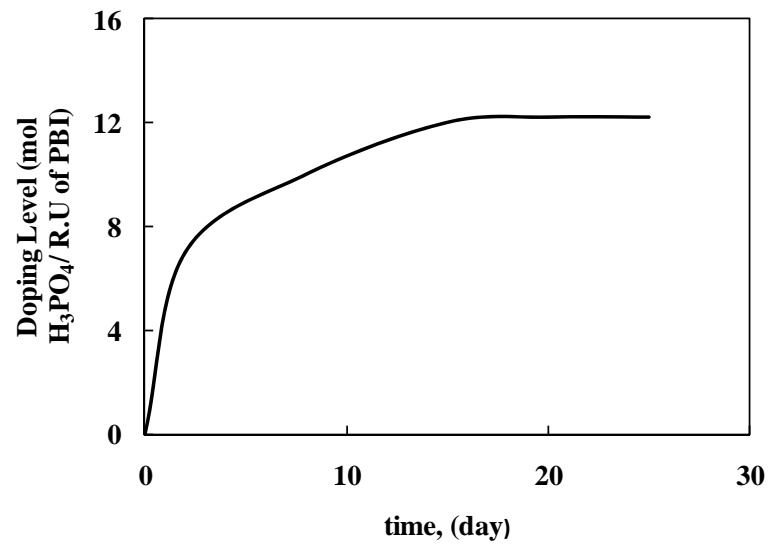


Figure A.1. Doping level changing by time

APPENDIX B

Sample Calculation of MEA Preparation

1. Gas diffusion layer is cut into 2.1cm*2.1 cm dimensions and weighed (X=tare of the GDL).

2. Catalyst solution is prepared. 20 wt % Pt/C is used as the catalyst and 0.4 mgPt/cm² loading on the electrode was aimed. The amounts of the contents are given below:

$$\text{Pt/C amount} = (0.4 \text{ mgPt/cm}^2) * (5 \text{ cm}^2) * (100 \text{ mg(Pt/C)/20mgPt}) / 1000 = 0.01 \text{ g Pt/C}$$

$$\text{Dry polymer amount} = (0.01) * (0.3) / (0.7) = 0.0043 \text{ g PBI}$$

$$\text{PBI solution amount (if the binder is only 5wt\% PBI solution)} \\ = (0.0043) * 100 / 5 = 0.0857 \text{ g PBI solution in DMAc}$$

3 times more than required amounts per 1 electrode to compensate the

losses arising from spraying;

0.03 g Pt/C (20%)

0.2571 g PBI solution (5%)

10 mL DMAc as solvent

3. These chemicals are mixed and then ultrasonicated for 2 hours and then sprayed onto the GDL by using spray gun and dried by a hot air gun.

4. Spraying was continued until the desired Pt loading was achieved: $X_{\text{final}} = X + (0.01) + (0.0043) \text{ g (after drying)}$.

5. Phosphoric acid doped PBI membrane is cut into 4cm*4cm dimensions.
6. Two electrodes are prepared in the same way and then they placed on two sides of the phosphoric acid doped PBI membrane. Then the MEA is hot pressed at 150°C and 250 psi.